

Challenges and Capabilities in Estimating Snow Mass Intercepted in Conifer Canopies with Tree Sway Monitoring

Mark S. Raleigh^{1,1}, Ethan D. Gutmann^{2,2}, John T Van Stan^{3,3}, Sean P. Burns^{4,4}, Peter D Blanken^{4,4}, and Eric E. Small^{4,4}

¹Oregon State University

²National Center for Atmospheric Research (UCAR)

³Georgia Southern University

⁴University of Colorado Boulder

November 30, 2022

Abstract

Snowpack accumulation in forested watersheds depends on the amount of snow intercepted in the canopy and its partitioning into sublimation, unloading, and melt. A lack of canopy snow measurements limits our ability to evaluate models that simulate canopy processes and predict snowpack and water supply. Here, we tested whether monitoring changes in wind-induced tree sway can enable snow interception detection and estimation of canopy snow water equivalent (SWE). We monitored hourly tree sway across six years based on 12 Hz accelerometer observations on two subalpine conifer trees in Colorado. We developed an approach to distinguish changes in sway frequency due to thermal effects on tree rigidity versus intercepted snow mass. Over 60% of days with canopy snow had a sway signal in the range of possible thermal effects. However, when tree sway decreased outside the range of thermal effects, canopy snow was present 93-95% of the time, as confirmed with classifications of PhenoCam imagery. Using sway tests, we converted significant changes in sway to canopy SWE, which was correlated with total snowstorm amounts from a nearby SNOTEL site (Spearman $r=0.72$ to 0.80 , $p<0.001$). Greater canopy SWE was associated with storm temperatures between -7 C and 0 C and wind speeds less than 4 m/s. Lower canopy SWE prevailed in storms with lower temperatures and higher wind speeds. We conclude that monitoring tree sway is a viable approach for quantifying canopy SWE, but challenges remain in converting changes in sway to mass and further distinguishing thermal and mass effects on tree sway.

1 **Challenges and Capabilities in Estimating Snow Mass Intercepted in Conifer**
2 **Canopies with Tree Sway Monitoring**

3
4 **Mark S. Raleigh¹, Ethan D. Gutmann², John T. Van Stan II³, Sean P. Burns^{2,4}, Peter D.**
5 **Blanken⁴, and Eric E. Small⁵**

6 ¹College of Earth, Ocean, and Atmospheric Sciences, Oregon State University, Corvallis, OR,
7 USA.

8 ²National Center for Atmospheric Research, Boulder, CO, USA.

9 ³Department of Biological, Geological, and Environmental Sciences, Cleveland State University,
10 Cleveland, OH, USA.

11 ⁴Department of Geography, University of Colorado, Boulder, CO, USA.

12 ⁵Department of Geological Sciences, University of Colorado, Boulder, CO, USA.

13
14 Corresponding author: Mark Raleigh (raleigma@oregonstate.edu)

15
16 Submitted to: *Water Resources Research*

17
18 **Key Points:**

- 19 • Six years of tree sway data from accelerometers on two conifers revealed changes in
20 sway frequency at sub-daily to seasonal scales
- 21 • After accounting for thaw-freeze cycles, changes in tree sway due to snow interception
22 were detected and checked with time-lapse images
- 23 • Sway data yielded canopy snow mass estimates consistent with snowfall data and storm
24 conditions

25 **Key Words:**

26 snow interception; tree sway; coniferous forests; accelerometers; time-lapse imagery

27
28 **Index Terms:** 0736, 0794, 1985, 1863, 3354

29 **Abstract**

30 Snowpack accumulation in forested watersheds depends on the amount of snow intercepted in
31 the canopy and its partitioning into sublimation, unloading, and melt. A lack of canopy snow
32 measurements limits our ability to evaluate models that simulate canopy processes and predict
33 snowpack and water supply. Here, we tested whether monitoring changes in wind-induced tree
34 sway can enable snow interception detection and estimation of canopy snow water equivalent
35 (SWE). We monitored hourly tree sway across six years based on 12 Hz accelerometer
36 observations on two subalpine conifer trees in Colorado. We developed an approach to
37 distinguish changes in sway frequency due to thermal effects on tree rigidity versus intercepted
38 snow mass. Over 60% of days with canopy snow had a sway signal in the range of possible
39 thermal effects. However, when tree sway decreased outside the range of thermal effects, canopy
40 snow was present 93-95% of the time, as confirmed with classifications of PhenoCam imagery.
41 Using sway tests, we converted significant changes in sway to canopy SWE, which was
42 correlated with total snowstorm amounts from a nearby SNOTEL site (Spearman $r=0.72$ to 0.80 ,
43 $p<0.001$). Greater canopy SWE was associated with storm temperatures between -7°C and 0°C
44 and wind speeds less than 4 m s^{-1} . Lower canopy SWE prevailed in storms with lower
45 temperatures and higher wind speeds. We conclude that monitoring tree sway is a viable
46 approach for quantifying canopy SWE, but challenges remain in converting changes in sway to
47 mass and further distinguishing thermal and mass effects on tree sway.

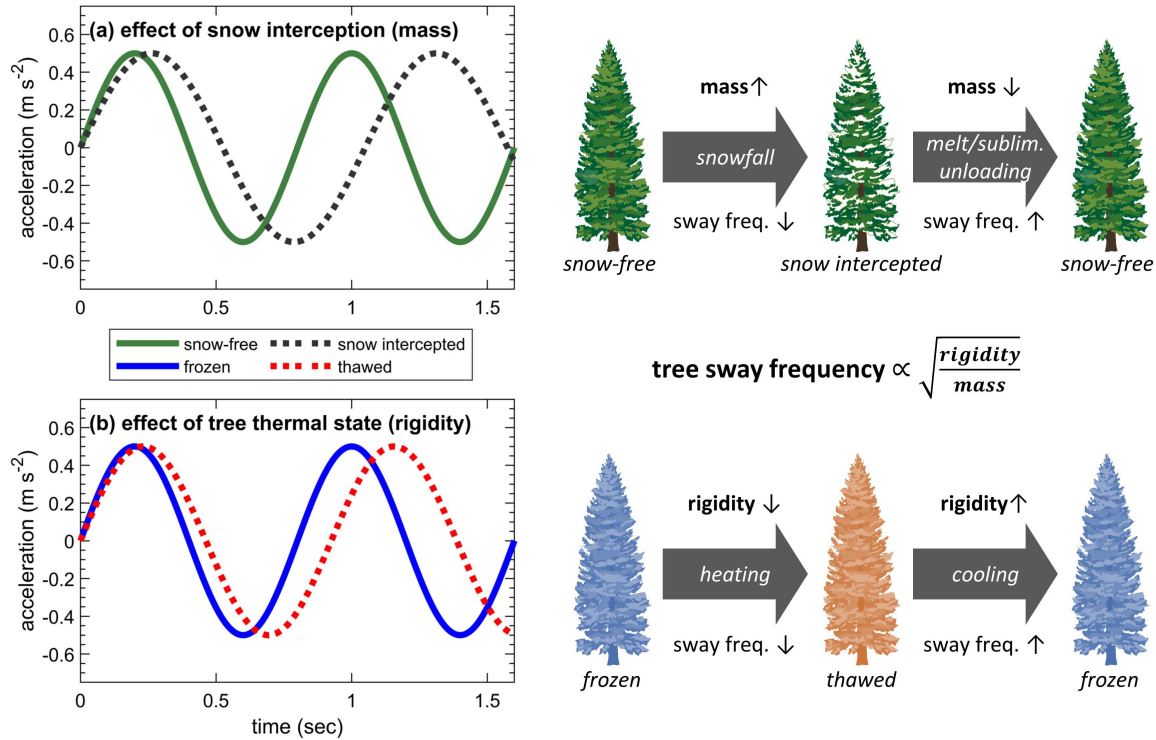
48 **1 Introduction**

49 Much of the global seasonal snow zone overlaps forests, which modify hydrological
50 processes and water availability (Essery et al., 2009; Rutter et al., 2009). In forests, snowpack
51 accumulation depends on the amount of snowfall intercepted in the canopy, and the fate of that
52 snow (i.e., sublimation, unloading, melt drip). Coniferous canopies may intercept more than 50%
53 of annual snowfall and reduce snow depth by a similar amount (Hedstrom & Pomeroy, 1998; Lv
54 & Pomeroy, 2020; Martin et al., 2013; John W. Pomeroy & Schmidt, 1993; Storck et al., 2002).
55 Increasing forest density influences not only snow accumulation, but also snowmelt processes
56 (Musselman et al., 2008; Varhola et al., 2010), the timing of which is ecologically significant and
57 dependent on climate (Dickerson-Lange et al., 2017; Lundquist et al., 2013). Thus, knowledge of
58 canopy snow processes is important for understanding and predicting the coupling between
59 forests and the snowpack, an enduring interest to watershed management (Church, 1912).

60 Reliably quantifying canopy snow interception is an outstanding challenge. A variety of
61 techniques have been tested (Friesen et al., 2015; Kinar & Pomeroy, 2015): measuring branch
62 deflection (Schmidt & Pomeroy, 1990), bagging and weighing intercepted snow on branches
63 (Schmidt & Gluns, 1991), weighing whole trees (Hedstrom & Pomeroy, 1998; Montesi et al.,
64 2004; Nakai et al., 1994; J.W. Pomeroy & Dion, 1996; Storck et al., 2002), and measuring trunk
65 compression (Martin et al., 2013; Van Stan et al., 2013). Although viable, these methods are not
66 commonly used due to substantial environmental disturbances, significant costs, or success in
67 only certain climates (c.f., Gutmann et al., 2017; Martin et al., 2013). Measuring snowfall
68 differences between adjacent forests and open areas can yield indirect estimates of interception
69 (Moeser et al., 2016; Roth & Nolin, 2019) but other processes complicate that approach.

70 Improved methods for monitoring canopy precipitation storage are needed to improve
71 understanding and prediction of forest hydrological processes (Friesen et al., 2015) and
72 interactions between canopy and the critical zone (Guswa et al., 2020). A low-cost and
73 minimally disruptive approach that can be applied across climates would provide new
74 opportunities to describe dynamics in canopy snow storage and advance model development.
75 Improved descriptions of canopy snow storage dynamics across sites are important to our efforts
76 to mitigate climate change impacts, as most model representations of snow interception are
77 attributed to two field studies (Hedstrom & Pomeroy, 1998; Storck et al., 2002) which diverge
78 when estimating snow interception capacity with warming temperature (Lundquist et al., 2021).
79 Representation of interception and unloading is a main factor leading to snow model divergence
80 in forested areas (Rutter et al., 2009). The field data needed to evaluate modeled snow
81 interception directly is non-existent in nearly all studies.

82 Monitoring changes to the natural sway frequency of a tree is a low-cost, non-intrusive,
83 and underexplored approach for quantifying canopy snow mass. Tree sway can be measured with
84 several sensors, such as accelerometers (Hassinen et al., 1998; Yang et al., 2021). Based on
85 mechanical theory (Figure 1), tree sway frequency varies with: (1) changes in mass (e.g., snow
86 interception), and (2) changes in rigidity (Bunce et al., 2019; Mayhead, 1973; Moore & Maguire,
87 2004). Using accelerometers on a spruce tree, Papesch (1984) measured a reduction in tree sway
88 frequency of 30% in a snow interception event, but did not quantify the mass of canopy snow or
89 effects of tree thermal state. Granucci et al. (2013) used clinometers to measure fluctuations in
90 tree sway as trees froze (more rigid) and thawed (less rigid), but excluded periods with canopy
91 snow. Freezing trees (Gutmann et al., 2017; Lindfors et al., 2019) and snowfall are concomitant
92 in cold climates; to our knowledge, no prior study has disentangled these effects on tree sway.



93
 94 **Figure 1.** Changes in tree sway frequency with (a) changes in mass due to snow interception and
 95 (b) changes in tree rigidity with thermal state (thaw-freeze cycle). The idealized time series (left)
 96 show lateral tree acceleration with wind-induced sway for cases of snow-free vs. snow
 97 intercepted and frozen vs. thawed state. Tree sway frequency can decrease as a tree intercepts
 98 snow (i.e., added mass) or as a frozen tree thaws (i.e., less rigid).

99 This “sway-to-mass” measurement concept was proposed to quantify rainfall interception
 100 (Friesen et al., 2015; Selker et al., 2011). Sway frequency has been found to decrease with
 101 increasing rainfall (van Emmerik et al., 2017). Beyond rainfall interception, tree sway is related
 102 to changes in biomass (e.g., tree health, phenology, water content and stress) and biosphere-
 103 atmospheric interactions (Baker, 1997; Ciruzzi & Loheide, 2019; van Emmerik et al., 2018;
 104 Gougherty et al., 2018; T. D. Jackson et al., 2021; Kooreman, 2013). Most studies have occurred
 105 in warmer conditions and have not needed to distinguish between mass and thermal effects on
 106 tree sway (Figure 1). Jackson et al. (2021) note “This could be particularly interesting in sites
 107 which freeze in winter since this will have a profound effect on the wood elasticity.”

108 The goal of this paper is to assess the feasibility of separating mass and thermal effects on
 109 tree sway, and demonstrate the potential for tree sway monitoring to enable quantification of
 110 canopy snow interception. We address two questions: (1) Can snow interception events be
 111 detected in tree sway time series? (2) How do sway-based estimates of canopy snow mass vary
 112 as a function of snowstorm characteristics? In the process, we identify the main challenges for
 113 this type of monitoring and highlight potential paths forward for improving this approach.

114 We monitored wind-induced movement of two trees with accelerometers for six years
 115 (2014-2020) in a coniferous forest of the Colorado Rocky Mountains. From these data, we derive
 116 hourly tree sway frequency and attempt to isolate tree sway variations due to thermal effects.
 117 Changes in tree sway unexplained by thermal effects enable snow interception detection. We
 118 also propose and test an empirical method for converting changes in sway to canopy snow mass.

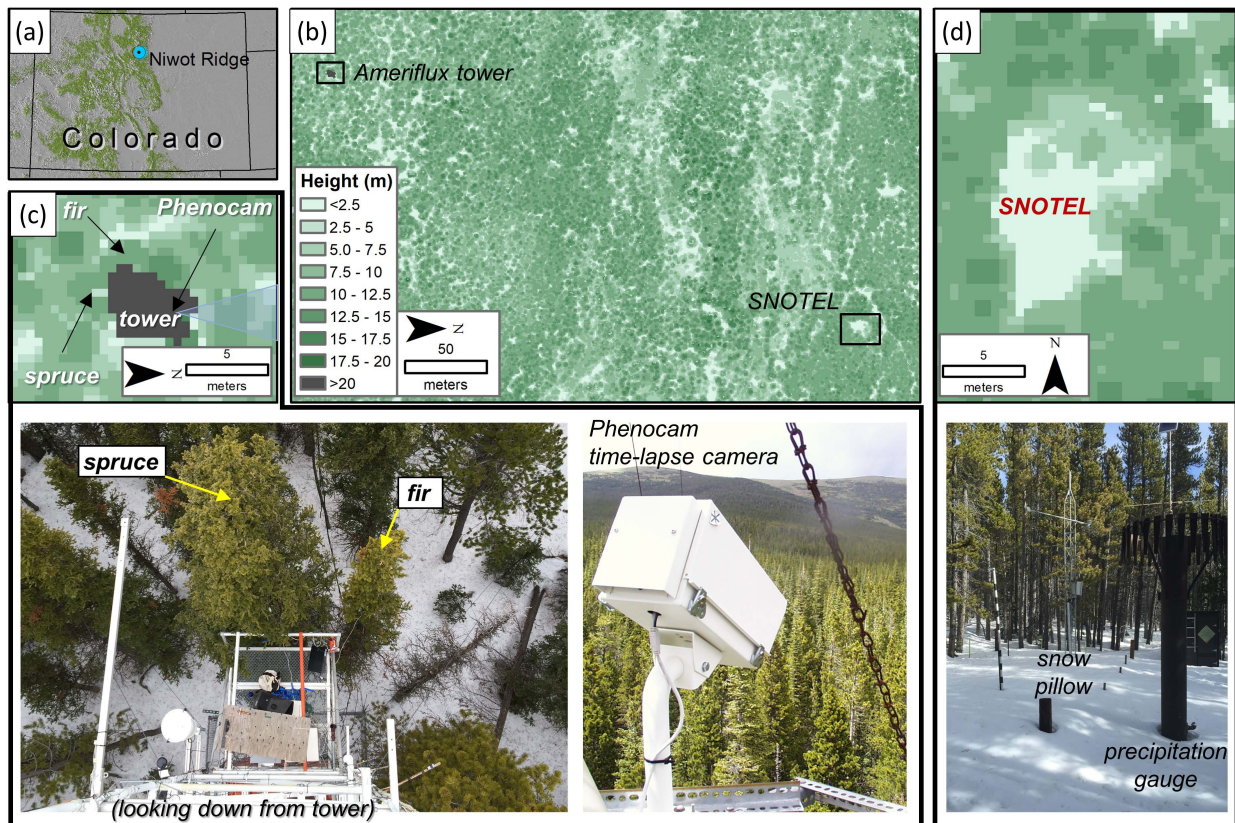
119 **2 Study Site, Sensors, and Data**

120 2.1 Study sites and tree characteristics

121 We monitored tree sway from November 2014 – August 2020 in a subalpine coniferous
 122 forest near the Niwot Ridge Long-Term Ecological Research (LTER) site in the Colorado Front
 123 Range, USA (Figure 2a). The C-1 site (N40.033, W105.547) is located at 3050 m elevation.
 124 Above-canopy wind speed averaged 5.2 m s^{-1} during the snow season (October-May), while
 125 mid-winter (December-February) air temperature averaged $-6.5 \text{ }^\circ\text{C}$. This was an ideal study site,
 126 given ample winds to activate tree motion, available scientific infrastructure, and prior forest
 127 research (e.g., Bowling et al., 2018; Gutmann et al., 2017; Molotch et al., 2007).

128 We instrumented two trees adjacent to the Niwot Ridge Subalpine Forest (US-NR1)
 129 AmeriFlux tower (Figure 2): a *Picea engelmannii* (engelmann spruce) and an *Abies lasiocarpa*
 130 (subalpine fir). These trees were selected because they represented two of the dominant species
 131 in the forest (Turnipseed et al., 2002), and because they were accessible from a tower platform
 132 next to the canopy edge (Fig. 2c). This platform did not impede tree motion.

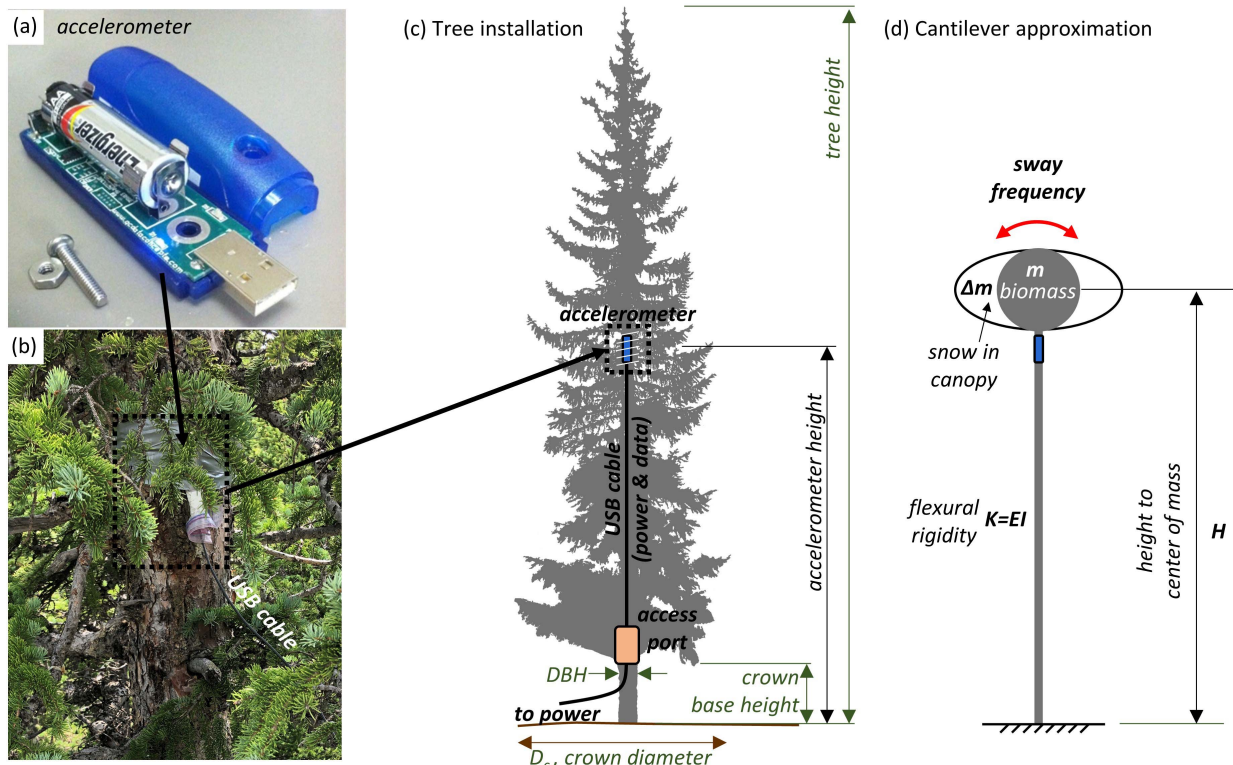
133 The forest in the vicinity of the tower has trees aged in the 100-250 year range (S P
 134 Burns, 2018). Tree height is typically around 10-15 m (Fig. 2b), with a mean canopy gap fraction
 135 of 17% and a leaf area index of 3.8 to $4.2 \text{ m}^2 \text{ m}^{-2}$ (Turnipseed et al., 2002). The study trees were
 136 in close proximity to each other but not close enough for crown collisions (Fig. 2c). Tree height
 137 was 13.0 m for the spruce and 11.0 m for the fir. Diameter at breast height (DBH) was 35.7 cm
 138 for the spruce and 18.5 cm for the fir. Based on the average of multiple radial measurements
 139 from canopy edge to bole, the effective crown diameter (D_c) was 3.4 m for the spruce and 1.7 m
 140 for the fir.



142 **Figure 2.** Study site maps and photos. (a) Map of Niwot Ridge in Colorado, with green regions
 143 mapping forests. (b) Tree height map showing locations of the AmeriFlux tower and SNOTEL
 144 site in a forest gap, with (c-d) zoomed maps and photos. Tree height maps are derived from an
 145 airborne lidar survey (Harpold et al., 2014) and gridded at 0.5 m resolution. Note north is to the
 146 right in (b) and (c) but up in (d).

147 2.2. Accelerometers and acceleration measurements

148 On each tree bole, we installed a single three-axis accelerometer to record acceleration
 149 associated with wind-induced tree movement (Figure 3). Installation heights were 8.9 m on the
 150 spruce and 8.1 m on the fir. Both accelerometers were Gulf Coast Data Concepts (GCDC) model
 151 X16-1D. Evans et al. (2014) compared multiple accelerometers and found GCDC had minimal
 152 noise but an uneven sampling rate. Therefore, we processed acceleration data using a frequency
 153 analysis for unevenly-sampled data (section 3.2). Prior to installation, we conducted a three-axis
 154 tumble test where the sensors were systematically rotated to ensure each axis recorded gravity
 155 when oriented downward. An installed USB extension cable provided external power to the
 156 sensor, enabled data download, and permitted sensor programming at an access port without
 157 disturbing the sensor (Figure 3). Each accelerometer logged three-axis acceleration data at ~12
 158 Hz nearly continuously over the study, yielding an 83 GB data volume total for both trees
 159 (Raleigh, 2021b, 2021a). Total cost of materials was about \$125 USD per installation. Further
 160 details are in Text S1.
 161



162 **Figure 3.** (a) GCDC accelerometer with cover removed. (b) Accelerometer installation on the
 163 spruce bole. (c) Conceptual installation and measurements. (d) Approximation of the tree as a
 164 cantilever with biomass (m), a transient snow load (Δm), and tree flexural rigidity (K) defined by
 165 modulus of elasticity (E) and area moment of inertia (I).
 166

167 2.3. Time-lapse imagery and canopy snow classification

168 A time-lapse camera enabled independent documentation of snow interception (Fig. 2c).
169 Camera images were acquired from the PhenoCam network (Richardson et al., 2018),
170 specifically camera “niwot2” before July 2015 and camera “niwot3” after July 2015. The camera
171 models were StarDot NetCam XL for niwot2 and StarDot NetCam SC for niwot3. Although the
172 cameras pointed away from the study trees (Fig. 2c), snow loading and unloading was consistent
173 on trees around the tower, based on independent field and camera observations (no data shown).

174 We manually classified daily canopy snow presence by examining up to four PhenoCam
175 images per day (8 AM, 11 AM, 2 PM, 5 PM); if any of those images showed canopy snow, that
176 day was recorded as having snow interception. While many images were unambiguous in the
177 classification, there were cases with modest amounts of canopy snow (e.g., light dusting of snow
178 or sporadic clumps persisting in time); we recorded these as snow interception days. In separate
179 analyses (not shown) we tested automated classifiers (i.e., machine learning, pixel thresholding)
180 but these were inconsistent relative to manual classifications.

181 2.4. Meteorology, tree temperature, and snowfall data

182 The study trees were located next to the US-NR1 AmeriFlux tower (Fig. 2c), which
183 included measurements of the local meteorological conditions (S. P. Burns et al., 2015). We used
184 wind speed (Campbell Scientific CSAT3 Sonic anemometer, 21 m height), relative humidity and
185 air temperature (Vaisala HMP-35D, 8 m height), and atmospheric pressure (Vaisala PTB-101B,
186 12 m height) to characterize storm conditions (see Text S2).

187 To isolate thermal effects on tree sway, we modeled tree sway as a function of
188 temperature (section 3.3) based on local tree bole temperatures (S. P. Burns et al., 2015;
189 Turnipseed et al., 2002). Bole temperatures were collected with Campbell A3537 (T-type
190 Thermocouples) sensors at 2 cm depth. Bole temperature data were missing prior to fall 2015,
191 and were thus unavailable in the first study year. For periods when bole temperatures were
192 unavailable, we substituted smoothed air temperature as a proxy (Lindfors et al., 2019), which
193 lags bole temperatures (Bowling et al., 2018; Sean P. Burns et al., 2018; Silins et al., 2000). Both
194 bole and air temperature were aggregated from 30-min to hourly values using a cubic smoothing
195 spline (“fit.m” in Matlab). Air temperatures were further smoothed with a 36-hour moving
196 average window, which yielded similar variance as winter bole temperatures.

197 The study area included a nearby NRCS SNOW TELEmetry (SNOTEL) station, located
198 in a ~10 m forest gap 360 m northeast and 20 m below the study site (Fig. 2b,d). We used hourly
199 SNOTEL snow water equivalent (SWE) data to assess the snowstorm magnitudes, for
200 comparison to the sway-to-mass approach. We quality controlled and filtered hourly SWE data
201 and then took all positive increments of hourly SWE as snowfall amounts. For each storm, the
202 total snowfall was determined as the sum of all hourly snowfall from the start to end of the
203 interception event, as detected in the sway data. We checked the snowfall derived from the
204 SNOTEL SWE against data from two nearby precipitation gauges (1) at the same SNOTEL site
205 (Fig. 2d) and (2) at the “Hills Mill” U.S. Climate Reference Network (USCRN) site, located in a
206 more exposed area outside the forest 400 m to the east and 30 m below the study site. Winter
207 SNOTEL precipitation was typically within 5% of SWE-derived snowfall amounts, while the
208 USCRN data typically had 40% less winter precipitation than both SNOTEL datasets. We
209 therefore used hourly snowfall derived from SNOTEL SWE to quantify storm totals.

210 3 Theory and Methods

211 3.1. Mechanical theory

212 When subject to a wind gust, a coniferous tree sways in a manner characteristic of a
 213 damped harmonic oscillator, e.g., a vertical cantilever beam (Fig. 3d) (Blevins, 1979; Bunce et
 214 al., 2019; Dargahi et al., 2020; Gardiner, 1992; T. Jackson et al., 2019; Moore & Maguire, 2004;
 215 Peltola, 1996; Pivato et al., 2014). In this approximation, the natural sway frequency (f , Hz)
 216 depends on its mechanical, geometric, and mass properties:

$$218 f \propto \frac{1}{2\pi} \sqrt{\frac{K}{m}} \quad (1)$$

219 where K is the flexural rigidity (or stiffness) and m is the total mass of the tree, including
 220 biomass and canopy water storage. Sway frequency (f) in Equation 1 is independent of wind
 221 speed, as long as there is sufficient wind to activate tree motion (see Text S2 and Figure S5). A
 222 tree may have multiple natural sway frequencies, but the first natural frequency dominates the
 223 sway response of a tree (Moore & Maguire, 2004) and is thus our focus.

224 In Equation 1, rigidity is the product of Young's modulus of elasticity (E ; mechanical
 225 property) and the area moment of inertia (I , geometric property); $K=EI$. E is a measure of
 226 resistance to elastic deformation per unit stress; a higher value signifies a more rigid tree. I
 227 depends on the cross-sectional geometry of the tree and is inversely related to tree diameter. E
 228 data for standing trees are scarce (Friesen et al., 2015) and were not measured here. Green wood
 229 E values are available in handbooks (USDA Forest Service, 2010) with nominal values of 7100-
 230 8600 MPa for engelmann spruce and 7200-8700 MPa for subalpine fir. However, our approach
 231 did not require an estimate of E , as we empirically related changes in f to changes in m while
 232 accounting for temperature effects on K (see sections 3.3-3.4).
 233

234 Both components of tree rigidity (E and I) vary with temperature and moisture content,
 235 especially in transitions between freezing and thawing states (Charrier et al., 2014, 2017; Gao et
 236 al., 2015; Gerhards, 1982; Green & Evans, 2008; Onwona-Agyeman et al., 1995; Sun et al.,
 237 2019). When temperatures are below the freezing point, the xylem of trees can freeze (e.g.,
 238 Bowling et al., 2018; Charrier et al., 2014, 2017; Gutmann et al., 2017). Freezing of tree xylem
 239 results in two opposing effects: (1) an increase in E (Gerhards, 1982; Green et al., 1999; Green &
 240 Evans, 2008; Lindfors et al., 2019; Silins et al., 2000), and (2) a decrease in I due to a shrinkage
 241 in tree diameter (Charrier et al., 2017; Lindfors et al., 2019). Observational studies show that tree
 242 sway frequency increases under freezing conditions relative to thawed conditions (Granucci et
 243 al., 2013), suggesting that the increase in E dominates the thermal effect on tree sway.

244 3.2. Frequency analysis of acceleration data

245 To obtain hourly time series of observed tree sway frequency (f_{obs}), we conducted
 246 frequency analyses on the 12 Hz data from the two lateral axes (N-S and E-W) of the
 247 accelerometers (section 2.2). We excluded the vertical axis data which were less sensitive to tree
 248 motion and had less consistent sway information. Data processing included three main steps: (1)
 249 frequency analysis, (2) filtering, and (3) smoothing.

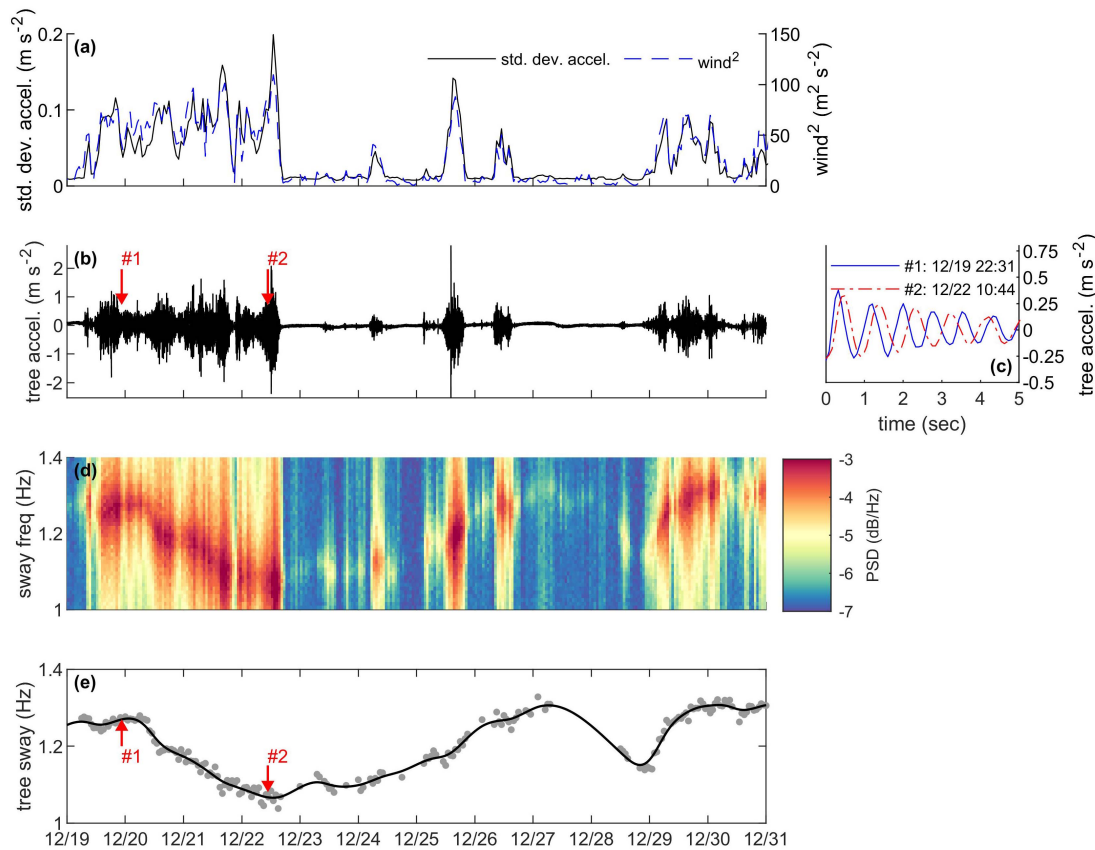
250 *Step 1.* Frequency analysis was conducted on each lateral axis using a non-overlapping
 251 sliding window of 1 hour, such that ~45000 acceleration data were analyzed to identify one sway

252 frequency value each hour. This window was short enough to resolve snow interception events
 253 while reducing noise relative to a shorter window (Text S3, Figures S7-S8). We used the Lomb-
 254 Scargle Periodogram (Lomb 1976; Scargle 1982), which yields Fourier-like estimates of power
 255 spectral density (PSD) for an unevenly sampled signal (section 2.2). In each window, we
 256 detrended the acceleration data, and then implemented the Lomb-Scargle analysis using Matlab
 257 (function “plomb.m”), with an oversampling factor of 2 and a maximum frequency of 3 Hz. The
 258 hourly tree sway frequency (Hz) was the frequency value with maximum PSD. We did not
 259 analyze other metrics such as frequency spectrum slope (van Emmerik et al., 2017).

260 *Step 2.* Hourly frequency data were filtered by removing any data that did not meet a
 261 minimum power level threshold of 0.99 (i.e., probability test of a true signal) and any outliers
 262 (i.e., 3 standard deviations) relative to the mean sway frequency in a sliding 72-hour window.

263 *Step 3.* To fill gaps in the time series, we smoothed sway frequency using splines with a
 264 smoothing parameter of 0.99. Smoothed sway frequency was highly correlated between axes
 265 ($r=0.93$ for spruce axes, $r=0.98$ for fir axes, not shown). Therefore, for each tree, we averaged the
 266 hourly smoothed sway frequency between the lateral axes for use in subsequent analyses.

267 Data processing for a 12-day example is illustrated in Figure 4. This shows that variations
 268 in tree motion scale with wind speed (Fig. 4a and Figure S6), but tree sway frequency does not
 269 vary with wind speed (Fig. 4e and Figure S5). In this 12-day interval, tree sway frequency was
 270 reduced on 22 December and 28 December, relative to ambient values. These occurred due to
 271 transient changes in either mass (e.g., snow interception) or tree rigidity (e.g., tree thaw).



272
 273 **Figure 4.** Example of measured and processed data for the east-west axis on the spruce tree in
 274 late December 2019. (a) Squared wind speed and hourly standard deviation in tree acceleration,
 275 showing tree motion scaling with wind energy. Measured 12 Hz tree acceleration over (b) the 12

276 day interval and (c) zoomed into two example sway events displayed over a 5 second interval.
 277 Event #2 had fewer sway cycles (~5.5 cycles) than event #1 (~6.5 cycles). (d) Hourly Lomb-
 278 Scargle power spectral density (PSD) displayed as a spectrogram, which shows the strength of
 279 frequencies in each hourly window. (e) Hourly tree sway, taken as the frequency with the
 280 maximum PSD in each hourly window (gray circles), and then filtered and smoothed to fill gaps
 281 (black line). Tree sway decreased from 1.27 Hz in event #1 to 1.08 Hz in event #2.

282 3.3. Distinguishing changes in sway frequency: thermal vs. mass effects

283 We assumed temporal changes in coniferous tree sway through the snow season
 284 (October-May) were due to either (1) gains/losses of water mass (i.e., snow) in the canopy, or (2)
 285 changes in rigidity due to thermal state (Figure 1) or a combination thereof. Thus, we
 286 hypothesized that controlling for changes in rigidity would reveal the incidence and magnitude
 287 of snow interception. We neglected other factors that can influence tree sway, such as changes in
 288 moisture content (likely more important in the growing season) and variations in the vertical
 289 center of mass due to uneven snow loading and unloading (see discussion). Changes in sway due
 290 to annual tree growth were accounted for implicitly by analyzing each year separately.

291 We assumed observed sway frequency (f_{obs}) had two components: (1) an unloaded sway
 292 frequency (f_0) that varied only with temperature and assumed a snow-free canopy, and (2)
 293 intermittent changes in sway (Δf) which were due to snow interception:

$$294 \quad 295 \quad 296 \quad f_{obs} = f_0(T) - \Delta f \quad (2)$$

297 Therefore, in snow-free periods, $\Delta f=0$, and thus $f_{obs} = f_0$. In periods with snow interception, we
 298 expected positive differences between f_0 and f_{obs} :

$$299 \quad 300 \quad 301 \quad \Delta f = f_0(T) - f_{obs} \quad (3)$$

302 Computing Equation 3 required a dynamic estimate of the unloaded sway frequency with
 303 temperature. We assumed this temperature-dependency was driven by changes in E , which
 304 increases as temperature decreases, with a sharper transition near the freezing point, and more
 305 modest changes at higher ($>5^\circ\text{C}$) and lower ($<-5^\circ\text{C}$) temperatures (Bowling et al., 2018; Gao et
 306 al., 2013, 2015; Green & Evans, 2008; Schmidt & Pomeroy, 1990; Silins et al., 2000; Sun et al.,
 307 2019). We represented this relationship as a sloped sigmoidal curve:

$$308 \quad 309 \quad 310 \quad f_0(T) = \frac{a-c}{1+e^{(-Tb-d)}} + c - hT \quad (4)$$

311 where a is a characteristic sway frequency (Hz) when frozen, b is a scaling parameter ($^\circ\text{C}^{-1}$)
 312 controlling the slope through the freeze-thaw zone, c is a characteristic sway frequency (Hz)
 313 when thawed, d is a shifting parameter accounting for temperature bias, T is temperature (air
 314 temperature, T_a , for WY 2015 and bole temperature, T_b for WY 2016-2020), and h is a slope
 315 parameter that permits sway to decrease linearly with T outside the freeze-thaw zone.

316 We fit and evaluated Equation 4 separately for each tree and year (Text S4). In each year,
 317 we randomly selected training points ($n=1000$ hours) when the PhenoCam imagery showed
 318 snow-free canopy, and fit Equation 4 to the hourly observed sway (f_{obs}) data. We used bole
 319 temperatures in water years (WY) 2016-2020, and 36-hour air temperatures in WY 2015 (when

320 bole temperatures were unavailable), and compared the fit statistics when both temperature
 321 datasets were available (Text S4, Figures S9-S10, Tables S2-S3).

322 When f_{obs} decreased significantly below f_0 (i.e., outside the range of thermal effects), we
 323 assumed snow was in the canopy and mass effects drove the decrease in tree sway. Detection of
 324 these events was achieved with the signal-to-noise ratio (SNR), a common metric for identifying
 325 meaningful information in a signal. SNR was calculated as Δf divided by the standard deviation
 326 of errors between estimated (f_0) and observed sway (f_{obs}) using the training points (see above).
 327 Standard deviation in sway error varied with both T_b and T_a , with the lowest variations at the
 328 lowest temperatures and the highest variations in error near $T_b=3^\circ\text{C}$ for the fir and $T_b=4^\circ\text{C}$ for the
 329 spruce (Figure S11); thus, SNR was temperature-dependent. For cases with $\Delta f > 0$, we identified
 330 snow interception when $\text{SNR} \geq 3$, which corresponds to a 1% probability of a false positive,
 331 assuming a normal distribution. When $\text{SNR} < 3$ or $\Delta f < 0$, we assumed thermal effects and mass
 332 effects cannot be distinguished in the sway data without independent information.

333 3.4. Evaluation of detected canopy snow

334 Applying the above thresholds for SNR and Δf yielded a sway-based estimate of when
 335 canopy snow was present. We evaluated this detection of canopy snow presence against
 336 PhenoCam imagery over the six snow seasons (1 October – 31 May). For this evaluation, we
 337 excluded the training points used to fit Equation 4, which enabled an independent assessment of
 338 canopy snow detection. We first aggregated the sway-based classifications of canopy snow
 339 (1=present, 0=absent) to daily values. We then computed standard commission and omission
 340 metrics of precision and recall, similar to snow mapping studies (e.g., Lv & Pomeroy, 2019;
 341 Raleigh et al., 2013):

$$343 \text{ Precision} = \frac{TP}{TP+FP} \quad (5)$$

$$345 \text{ Recall} = \frac{TP}{TP+FN} \quad (6)$$

346 where true positives (TP) had canopy snow in both datasets, false positives (FP) had canopy
 347 snow in the sway data only, and false negatives (FN) had canopy snow in the imagery only.
 348 Precision computed the fraction of days when canopy snow detected by sway was confirmed
 349 with the imagery. Recall computed the fraction of all days with canopy snow that were detected
 350 in the sway data.
 351

352 3.5. Estimating canopy SWE from decreases in tree sway frequency

353 We estimated canopy SWE from Δf after SNR filtering (section 3.3). To convert Δf to a
 354 change in mass (Δm), we conducted multiple sway tests at each tree to empirically define the
 355 relationship. In these tests (Fig. 5a), we induced sway by pulling on the unloaded tree ($\Delta m=0$)
 356 with a rope and suddenly releasing it (Mayhead, 1973) to produce swaying motion in both lateral
 357 directions. The accelerometer recorded acceleration while each tree was freely swaying (Fig. 5b),
 358 enabling identification of unloaded sway frequency (f_0). We then conducted a series of tests
 359 where we attached a known mass (Δm) to the bole, induced sway again, and recorded Δf relative
 360 to the first test with no mass in the canopy (Fig. 5b). We conducted tests with a range of masses
 361 up to 61 kg; heavier masses raised logistical and safety concerns. For a given Δm , we induced
 362 sway at least five times, and found the sway frequency across all trials.

363 Sway tests occurred under thawed conditions on four dates on both trees (September
 364 2015, December 2015, June 2016, October 2017), with a fifth test on the fir tree (February
 365 2016). Conducting tests under freezing conditions were too challenging. For each tree and test,
 366 the mass was placed at approximately the same height (i.e., ~7.5 m).

367 We fit a linear relationship (zero intercept) to the Δf and Δm data from the sway tests:

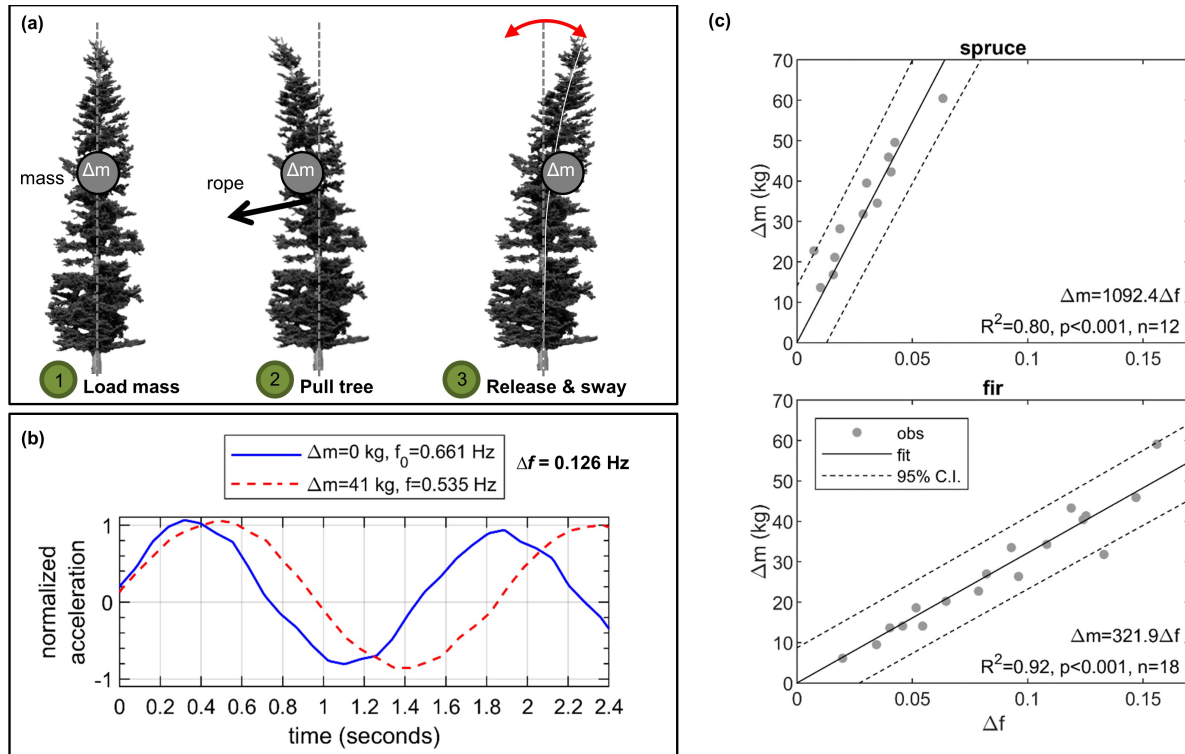
$$368 \Delta m = \alpha \times \Delta f \quad (7)$$

369 where α is a slope parameter (kg Hz^{-1}) that specifies that scaling of mass with a change in sway
 370 frequency. To characterize uncertainty, we computed 95% confidence intervals (C.I.) on α to
 371 account for measurement errors in Δm and Δf . The data and fit are shown in Figure 5c with more
 372 information in Text S5 and Table S4. The spruce had a steeper slope than the fir, presumably due
 373 to greater biomass. We were unable to test how the α slope might change with temperature and
 374 thermal changes in tree rigidity; see discussion for potential effects of this assumption.

375 Finally, we converted Δm to canopy SWE (mm) per unit area based on the vertical
 376 projected tree area (based on crown diameter D_c , Section 2.1), following Storck et al. (2002):

$$377 \text{SWE}_{can} = \frac{4\Delta m}{\pi D_c^2} \quad (8)$$

381

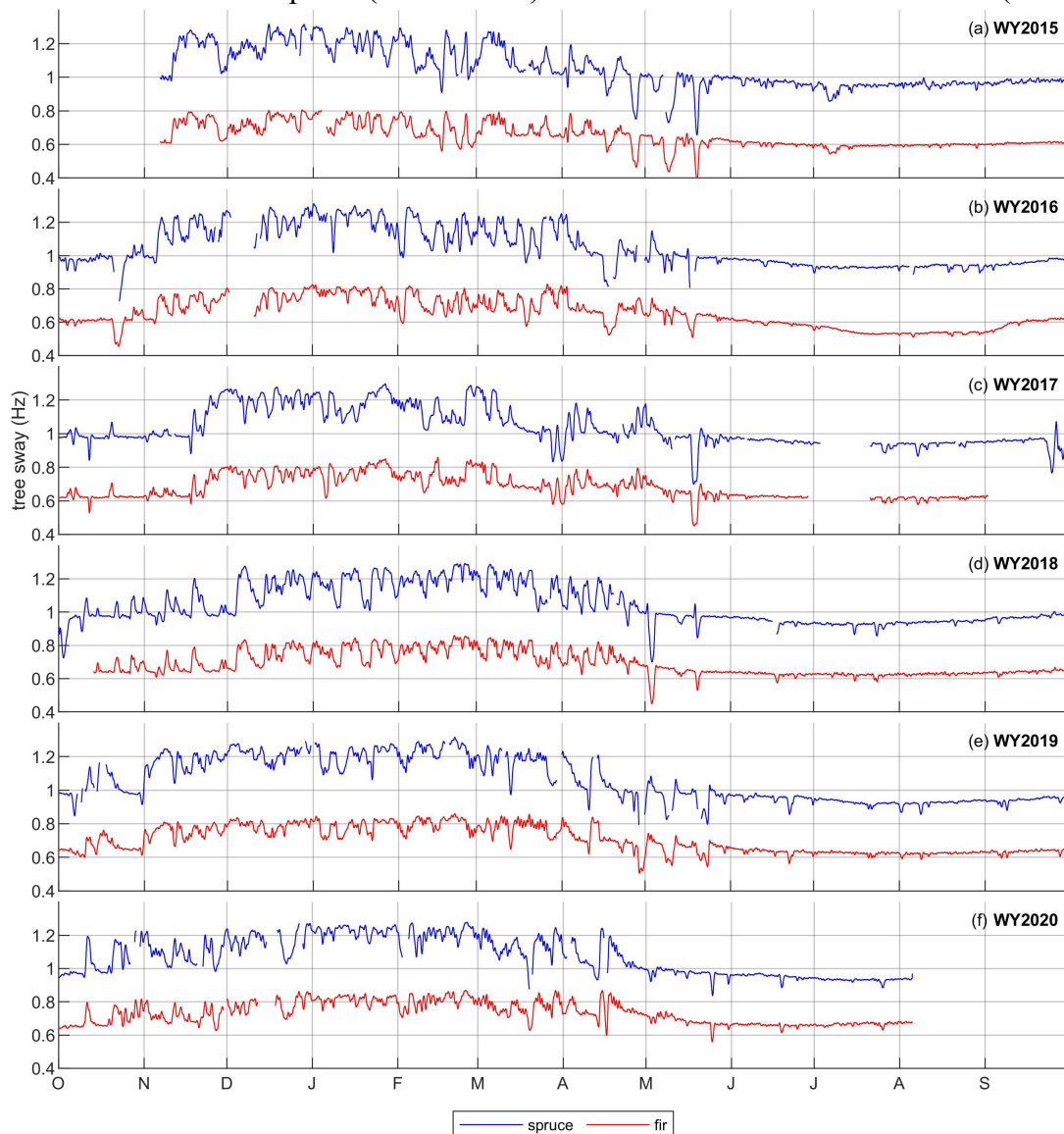


382 **Figure 5.** (a) Tree sway test, where a known mass (Δm) was fixed to the bole, the tree was pulled
 383 and released to induce sway. (b) Tree acceleration data (normalized) for two tests, including no
 384 added mass (blue line) and an added mass of 41 kg, which decreased sway by 0.126 Hz. (c)
 385 Derived relationships between decrease in sway (Δf) and added mass (Δm) for all tests conducted
 386 on the spruce and fir trees.
 387

388 **4 Results**

389 4.1. Tree sway variations

390 Time series of hourly tree sway were derived from the observed acceleration data on the
 391 spruce and fir trees over 2014-2020. Tree sway was significantly correlated between the two
 392 trees (Pearson correlation $r=0.92$, Figure 6). Tree sway varied seasonally, with higher frequency
 393 during winter and lower frequency during summer, with variations coinciding with temperature
 394 rather than wind speed (Text S2, Fig S5). Sway frequency declined until mid-summer and then
 395 increased through fall. Sporadic decreases in sway frequency were evident throughout the year,
 396 but were larger and more common in the snow season (October-May) than in the warm season
 397 (June-September). Decreases in sway frequency during summer were not analyzed but often
 398 coincided with rainfall (not shown). Over the six years, mean sway frequency increased from
 399 1.05 to 1.07 Hz for the spruce (2% increase) and from 0.65 to 0.73 Hz for the fir (12% increase).



400
 401
 402

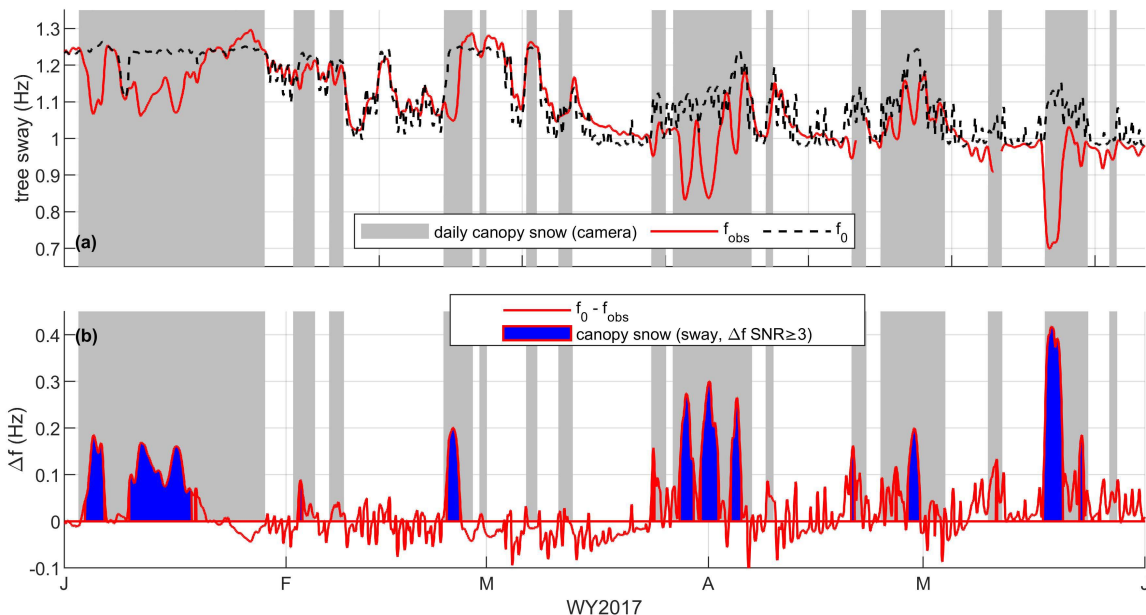
Figure 6. Observed hourly tree sway (Hz) derived from accelerometer data recorded on spruce and fir trees from water years 2015-2020 (a-f). Data gaps exceeding 1 day are omitted.

403 4.2. Distinguishing sway changes between thermal effects and snow interception

404 The modeled relationship between temperature and unloaded sway frequency (f_0) was
 405 evaluated (see Tables S2-S3). The R^2 ranged from 0.89-0.95 for the spruce and 0.71-0.87 for the
 406 fir, with root mean squared error (RMSE) ranging from 0.02-0.03 Hz for both trees. The standard
 407 deviation in f_0 residuals (for SNR calculations) varied with temperature, with the lowest value of
 408 0.02 Hz at -10°C for both trees, and the highest of 0.13 Hz (spruce) and 0.09 Hz (fir) around 3 to
 409 4°C . Analysis showed similar statistical fit for air and bole temperatures (see Text S4),
 410 supported the use of air temperature when bole temperatures were unavailable (i.e., WY 2015).

411 Comparing f_0 to observed sway (f_{obs}) allowed us to isolate when sway frequency was
 412 varying due to thermal effects. To illustrate, we highlight water year 2017 in Figure 7. Over
 413 many intervals, f_{obs} tracked f_0 (Fig. 7a), which suggested thermal effects drove those variations
 414 (e.g., sway decrease in mid-February). However, there were also multiple intervals when f_{obs}
 415 diverged from f_0 (e.g., three events near 1 April, one large event in mid-May). These often
 416 coincided with times when canopy snow was identified in the imagery (gray zones, Figure 7).

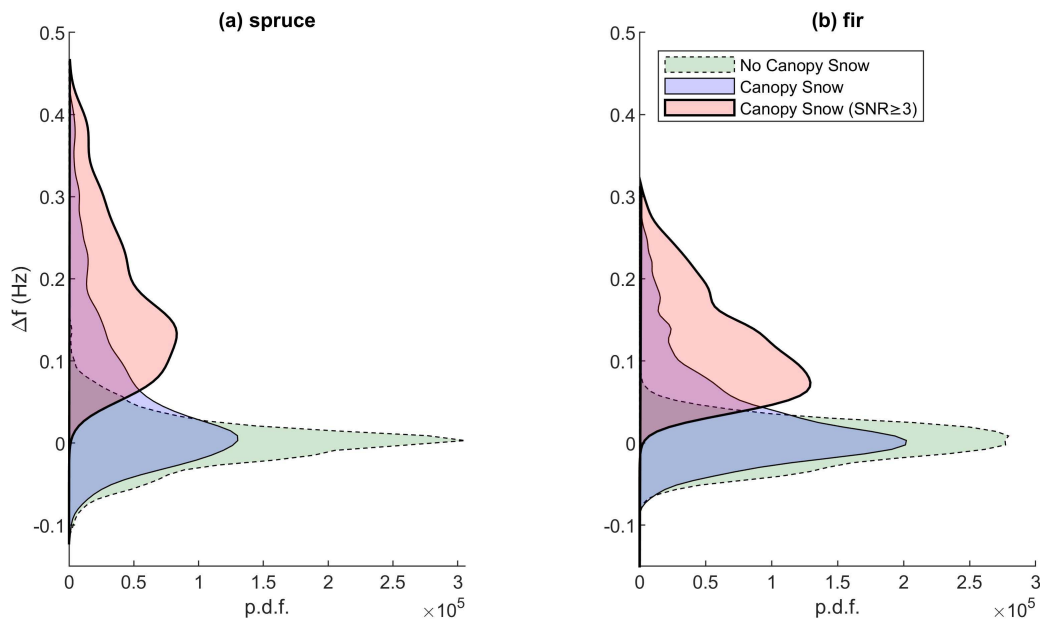
417 We computed Δf (Equation 3) by subtracting f_{obs} from f_0 , which clarified the magnitude
 418 and timing of decreases in sway frequency unexplained by thermal effects (Fig. 7b). Intervals
 419 when the Δf SNR ≥ 3 (highlighted in blue) were all coincident with times when the camera
 420 classification showed snow in the canopy. The magnitude of Δf varied seasonally, with higher Δf
 421 in the late fall and spring (e.g., May 2017), and more modest Δf in cold winter months (e.g.,
 422 January 2017). Some events with positive Δf did not meet the SNR ≥ 3 requirement for canopy
 423 snow detection; mass and thermal effects could not be distinguished in those cases (e.g., 7-8
 424 February). Note that in some periods the duration of canopy snow were overemphasized in the
 425 image analysis (e.g., most of January 2017) due to persistent, isolated clumps of canopy snow.



426
 427 **Figure 7.** (a) Hourly observed tree sway (f_{obs}) and unloaded tree sway (f_0) estimated from bole
 428 temperature and Equation 4. (b) Changes in sway frequency (i.e., differences between f_0 and f_{obs} ,
 429 Equation 3). Gray areas are intervals when daily classifications of time-lapse camera imagery
 430 showed snow in the canopy. The blue intervals are events when Δf SNR ≥ 3 and thus canopy snow
 431 is detected in the sway data. Example is from the spruce tree during water year 2017.

432

433 We assessed the detectability of canopy snow in the sway data. The distribution of Δf
 434 based on canopy snow presence or absence showed broad overlap at low values of Δf , typically
 435 less than 0.1 Hz (blue vs. green in Figure 8). However, larger values of Δf typically coincided
 436 with canopy snow. When constraining to intervals when the $\text{SNR} \geq 3$ threshold was enforced for
 437 canopy snow detection, distributions were more distinct (compare red vs. green in Figure 8). The
 438 precision metric for canopy snow detection (with $\text{SNR} \geq 3$) was 0.93 for the spruce and 0.95 for
 439 the fir, indicating that most days with canopy snow detected in the sway data were corroborated
 440 with image analysis. In contrast, the recall metric was 0.40 for the spruce and 0.36 for the fir,
 441 indicating that 60-64% of days with canopy snow (known from the imagery) were not detected
 442 in the sway data. The low recall was influenced by several intervals when the mass of canopy
 443 snow was minimal (e.g., dusting of snow in canopy or isolated snow clumps). Recall can be
 444 improved using a lower SNR threshold, but with a tradeoff of reduced precision (not shown).
 445



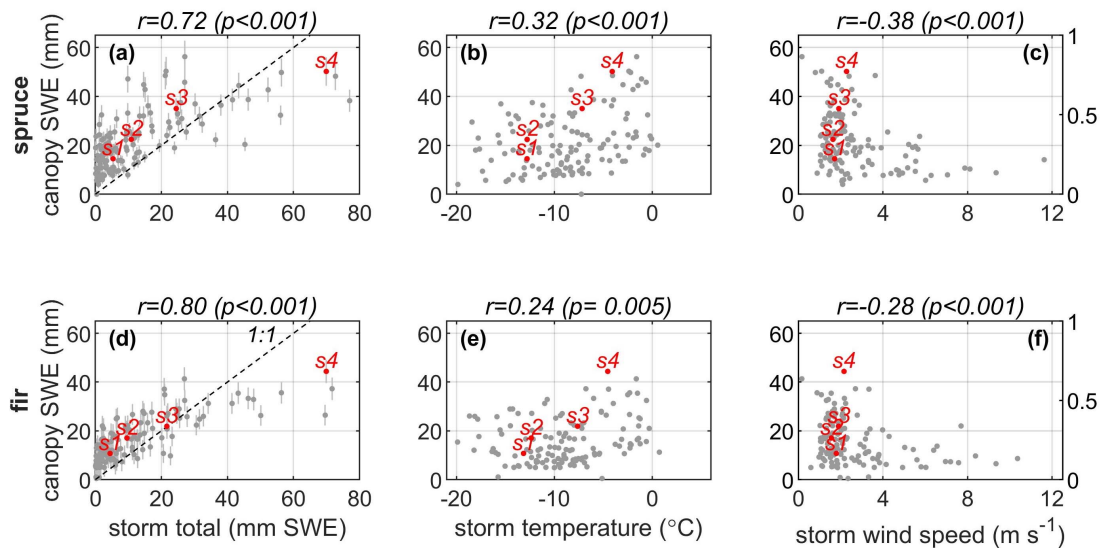
446 **Figure 8.** Probability distribution functions (pdfs) of Δf for the (a) spruce and (b) fir, with
 447 different distributions shown for intervals when canopy snow was absent or present, based on
 448 daily time-lapse camera classification. The canopy snow pdfs are separated for all points (blue)
 449 and only points exceeding the SNR detection limit (red).
 450

451 4.3. Estimating canopy SWE and contextualizing with snowstorm attributes

452 We next examined canopy SWE estimated from changes in tree sway frequency and
 453 compared those estimates to snowstorm magnitudes and characteristics (Figure 9). With the data,
 454 we identified and analyzed 137 snow interception events in the spruce data and 136 events in the
 455 fir data over the six year period, confirmed in both the tree sway data ($\Delta f > 0$ and $\text{SNR} \geq 3$) and
 456 PhenoCam images. The interception events analyzed for these neighboring trees were slightly
 457 different due to tree-to-tree differences in SNR. For each storm, we calculated the total snowfall
 458 (section 2.4), and mean wet bulb temperature, and mean wind speed. Changes in sway were
 459 converted to canopy SWE following Equations 7 and 8.

460 Both trees showed a general increase in canopy SWE with increasing storm totals (Fig.
 461 9a,d). Based on Spearman's ranked correlation between canopy SWE and storm totals, we
 462 calculated $r=0.72$ for the spruce and $r=0.80$ for the fir with $p<0.001$ for both trees. Images from
 463 four example storms (s1-s4) also qualitatively supported the general increase in canopy SWE
 464 with storm total (Figure 9). A wide range of storm totals produced a similar canopy SWE. For
 465 example, the 10 highest canopy SWE amounts (44-56 mm for the spruce, and 32-44 mm for the
 466 fir) coincided with storms ranging from 10 to 72 mm of snowfall (Fig. 9a,c). Note that many
 467 canopy SWE values exceeded the storm total (left of 1:1 line), suggesting a high bias in the
 468 sway-to-mass data, a low bias in the SNOTEL data or both. One of the largest interception
 469 events was in mid-May 2017, which was a 70 mm snowstorm that registered canopy SWE of 50
 470 mm on the spruce and 44 mm on the fir (s4 in Figure 9). Lower canopy SWE values (< 20 mm
 471 for both trees) were generally confined to storm totals less than 25 mm SWE.

472 Across storms, canopy SWE had significant but modest correlations with temperatures
 473 (Fig. 9b,e) and wind speeds (Fig. 9c,f). For both trees, the highest canopy SWE values were
 474 associated with temperatures between -7°C and 0°C and wind speeds less than 4 m s^{-1} . Lower
 475 canopy SWE values were found in storms with lower temperature storms and high wind speeds.



476
 477 **Figure 9.** Sway-to-mass maximum canopy SWE of the (top row) spruce tree ($n=137$ storms) and
 478 (middle row) fir tree ($n=136$ storms) for storms over WY 2015-2020. Canopy SWE versus storm

479 (a,d) total snowfall at the SNOTEL site, (b,e) mean wet bulb temperature, and (c,f) mean wind
480 speed. Error bars are shown in the snowfall comparison (a,d) based on the 95% confidence
481 interval from sway tests. Spearman's rank correlations coefficients and p-values are shown. Four
482 storms are labeled (s1-s4) with time-lapse images shown at the bottom, with dates: 28 December
483 2019 (s1), 22 January 2019 (s2), 1 May 2016 (s3), and 19 May 2017 (s4).

484 5 Discussion

485 We have tested the capability for extracting quantitative snow interception information
486 from time series of wind-induced tree sway, obtained from low-cost, non-destructive, and
487 relatively simple installations with accelerometers. Data analysis revealed sub-daily to seasonal
488 variations in sway frequency of two subalpine conifers (Figure 6), driven by intercepted snow
489 mass and changes in tree rigidity through thaw-freeze cycles and thermal fluctuations (Figure 1).
490 This paper has demonstrated the challenges and feasibility in disentangling these two drivers of
491 conifer sway variations (Figures 7-8), which can permit (1) detection of snow interception and
492 (2) quantitative estimates of canopy SWE across a range of storms (Figure 9), thereby addressing
493 the two study questions (section 1). The six year datasets may be among the longest canopy
494 snow records and the longest tree sway records, and are publicly available to support studies of
495 forest ecohydrology processes (Raleigh, 2021b, 2021a).

496 To our knowledge, this is one of the first attempts to consider the challenges associated
497 with applying the sway-to-mass method to measure snow intercepted in conifer canopies. The
498 main challenges for the snow interception application are: (1) developing reliable estimates of
499 tree sway due only to thermal effects (f_{θ}), (2) relating changes in tree sway (Δf) to changes in
500 mass (Δm), and (3) detecting and quantifying canopy snow during periods with low wind speeds.
501 All challenges except for the last one may be addressed in future research that uses
502 accelerometers; other techniques (e.g., stem compression) are necessary for measuring canopy
503 interception in low-wind conditions. Below, we discuss these challenges.

504 Reliable estimates of sway variations due to thermal state (i.e., thaw-freeze cycles) can be
505 developed with empirical relationships with temperature. When observed tree sway decreases
506 below the range of expected thermally-driven values, snow interception can be successfully
507 detected (Figures 7-8) with high precision scores (0.93-0.95). The model of f_{θ} generally showed
508 reasonable skill (R^2 typically from 0.71 to 0.95), with improved prediction for the spruce over
509 the fir, and similar skill when using bole temperature versus smoothed air temperature (Text S4).
510 Prior studies have also used air temperature to estimate dynamic tree properties with comparable
511 skill (e.g., Schmidt & Pomeroy, 1990). Improved predictions of unloaded sway might be possible
512 by accounting for hysteresis in thaw-freeze events (Sun et al., 2019) and with more detailed
513 models (Musselman & Pomeroy, 2017). We expect improved f_{θ} estimation will reduce the SNR
514 and improve detection of more modest snow interception events (i.e., improve the recall score).

515 Empirical sway tests were used to convert Δf to canopy SWE (Equations 7 and 8), but
516 this appeared to overestimate canopy SWE (see points above 1:1 line in Figure 9a,d) for multiple
517 reasons. First, we assumed mass was concentrated in one place in the canopy (Fig. 3d), which
518 was a simplification. Vertical distributions of canopy snow are complex and have variable center
519 of mass with dynamic loading and unloading. If intercepted snow has a higher center of mass
520 than the mass in our sway tests, that could cause a high bias in canopy SWE estimates. We did
521 not characterize the canopy snow center of mass, but that might be possible with terrestrial lidar
522 surveys (Russell et al., 2020). Second, sway tests were only conducted under thawed conditions,
523 and we could not assess the effect of rigidity on the conversion of Δf to canopy SWE. It is

524 possible that the α slope (i.e., dm/df) decreases with temperature; future sway tests could be
525 completed at colder temperatures to confirm. Given our tests were at warmer conditions than
526 many interception events, we likely overestimated canopy SWE at the coldest temperatures (i.e.,
527 highest f_0). Finally, we only tested with a modest mass (maximum near 60 kg). We extrapolated
528 to larger snow masses, which might further contribute to errors in canopy snow estimation. As an
529 alternative to empirical sway tests, a more mechanistic approach could yield canopy sway mass
530 estimates by accounting for all dynamic factors influencing tree sway variations, including the
531 height of intercepted snow, changes in biomass, variations in internal moisture content (Ciruzzi
532 & Loheide, 2019), and variables related to tree rigidity (modulus of elasticity, DBH).

533 Despite these challenges, this study showed that the methodology has capabilities for
534 improving hydrologic monitoring of snow in forested watersheds. First, the data revealed
535 realistic changes in canopy SWE, relative to storm characteristics. Second, the data have
536 implications for evaluating and refining modeled canopy snow processes.

537 We detected snow interception over a series of storms and found realistic relationships
538 between canopy SWE and storm characteristics. Canopy SWE was significantly associated with
539 storm SWE totals, but there were notable variations between storms (Figure 9) that were partially
540 explained by variations in (1) wind and (2) temperature (Gutmann, 2020). Storms with high wind
541 speeds can induce mechanical unloading and enhance sublimation; this is consistent with the
542 observed reduction in canopy SWE with increasing wind speed, especially above 4 m s^{-1} (Fig.
543 9c,f). To compare, Miller (1962) suggested snow interception decreases as wind speed exceeds 2
544 m s^{-1} . In addition to storms with low wind, higher canopy SWE was found in storms with higher
545 temperatures. Snow falling near the melting point is more cohesive and able to bridge conifer
546 needles to enhance interception capacity (Kobayashi, 1987; Schmidt & Gluns, 1991). Warming
547 temperature also reduces branch rigidity, which can induce sloughing of snow and decrease
548 canopy SWE (Schmidt & Pomeroy, 1990). The sway-to-mass data for both trees highlight a
549 collection of storms where the cohesion effect apparently prevails despite the potential for less
550 rigid branches (Fig. 9b,e).

551 Although we do not apply process-based models, canopy SWE estimates from the sway
552 data have potential to benefit snow and land surface model development, such as refining the
553 representation of maximum interception and the time scales of loading and unloading. Maximum
554 interception capacity is a common parameter in snow and land surface models (Gutmann, 2020;
555 Rutter et al., 2009) but the parameter has noted ambiguity (Lundquist et al., 2021). The sway-to-
556 mass estimates of canopy SWE suggest this model parameter (assuming one exists) would be at
557 least 56 mm for the spruce, and 44 mm for the fir (Figure 9), though these may be overestimated
558 due to limitations with the sway tests (see above). Likewise, maximum interception capacity
559 varies with temperature in models, with two common parameterizations showing opposing
560 temperature sensitivities, due to the processes discussed above (Lundquist et al., 2021). The
561 canopy-to-mass data could guide selection and development of an interception parameterization
562 that is most realistic for particular conditions.

563 The above interception capacity estimates are close to values found in the literature. For
564 example, Storck et al. (2002) reported maximum interception was at least 40 mm SWE for a
565 Douglas fir in Oregon. However, this was for a different conifer species and a different climate,
566 highlighting the problem with data sparsity and the need for more accessible canopy SWE data
567 in space. The 30% reduction in sway frequency of a Sitka spruce tree observed by Papesch
568 (1984) during a snow interception event falls within the range of our values (Figure 8).

569 In terms of limitations, this study was confined to two coniferous trees in a continental
570 climate, and lacked reference measurements of canopy SWE from more established techniques
571 (e.g., weighing trees). Future work is needed for these comparisons (Klamerus-Iwan et al., 2020).
572 The relative ease of sway measurements could enable longitudinal studies across trees (species
573 and sizes) and climates. The sway-to-mass approach appears viable across a range of thermal
574 states (Fig. 9b,e) and therefore may be a more universal approach than other techniques that have
575 only worked over a limited range of climate and temperature conditions (e.g. trunk compression).
576 However, the dependence of the sway-to-mass method on wind to activate tree motion may limit
577 its utility in locations and times with minimal wind. Additionally, availability of existing
578 infrastructure (e.g., an adjacent tower, Fig. 2) or the practicality and safety in tree climbing may
579 constrain selection of trees for instrumentation.

580 Finally, to increase the relevance of tree sway monitoring to forested watershed modeling
581 and management, there is a need to understand the spatial scaling of the time series data. The
582 high correlation between our two study trees ($r=0.92$, Figure 6) suggests continuous sway
583 monitoring might represent temporal variations across a forest stand. However, it is important to
584 contextualize the sway time series observed at one or more trees relative to the sway dynamics of
585 the greater stand. This upscaling could be achieved in multiple ways, such as mapping of sway
586 based on allometric data (Bunce et al., 2019; T. Jackson et al., 2019; T. D. Jackson et al., 2021;
587 Moore & Maguire, 2004; Sugden, 1962), or through resolving spatial sway variations with
588 video-based approaches (Enuş et al., 2020). However the challenges outlined above (estimating
589 f_0 and converting Δf to Δm) would need to be resolved at this larger scale.

590 **6 Conclusions**

591 Sub-daily to seasonal changes in tree sway frequency in a subalpine coniferous forest are
592 driven by snow interception events and changes in tree thermal state with freeze-thaw cycles. By
593 accounting for changes in tree thermal state, analysis of tree sway time series can enable
594 detection of the timing of snow interception events and estimation of canopy SWE. In turn, these
595 data provide novel characterization of interception dynamics between storms; such observations
596 are rarely available.

597 There is a growing suite of ecohydrological processes that can be characterized by
598 monitoring tree sway (T. D. Jackson et al., 2021); the present study has provided evidence for the
599 application with canopy snow interception. The relative ease, cost-effectiveness (as low as \$125
600 USD per installation), and non-destructive measurement approach of tree sway can be applied in
601 other studies of forest processes, thereby providing new avenues for model development, which
602 can inform resource management and environmental research. Nevertheless, several challenges
603 need to be resolved to better constrain the sway-based estimates of canopy SWE.

604 **Data Availability Statement**

605 All datasets used in this study are freely available in public repositories. Raw 12 Hz tree
606 acceleration data and hourly processed sway variables (Raleigh, 2021b, 2021a) are available for
607 the spruce tree at <https://doi.org/10.5281/zenodo.5130616> and for the fir tree at
608 <https://doi.org/10.5281/zenodo.5149308>. The US-NR1 AmeriFlux data are available at
609 <https://doi.org/10.17190/AMF/1246088> and at <https://doi.org/10.15485/1671825>. PhenoCam
610 imagery are available at <https://PhenoCam.sr.unh.edu/>. NRCS SNOTEL data are available at
611 <https://www.wcc.nrcs.usda.gov/snow/>.

612 **Acknowledgments**

613 M. Raleigh led the study with support from the National Science Foundation (NSF EAR Award
614 1761441), the Advanced Study Program (ASP) at NCAR, and the CIRES Visiting Fellow
615 program. The US-NR1 AmeriFlux site has been supported by the U.S. DOE, Office of Science
616 through the AmeriFlux Management Project (AMP) at Lawrence Berkeley National Laboratory
617 under Award Number 7094866. We thank Pablo Mendoza for manuscript discussions and field
618 assistance. We also acknowledge Dan Stern, Morgan Raleigh, and Coulee Raleigh for field
619 assistance, and Jeff Tecca for assistance with data archiving. The authors declare that they have
620 no real or perceived conflicts of interests, financially or institutionally, in the presented work.
621 NCAR is sponsored by the National Science Foundation. We thank the many collaborators,
622 including site PIs and technicians, for their efforts in support of PhenoCam.

623 **References**

- 624 Baker, C. J. (1997). Measurements of the natural frequencies of trees. *Journal of Experimental*
625 *Botany*, 48(5), 1125–1132. <https://doi.org/10.1093/jxb/48.5.1125>
- 626 Blevins, R. D. (1979). *Formulas for natural frequency and mode shape*. New York, NY: Van
627 Nostrand Reinhold Co. [https://doi.org/10.1016/0301-679x\(80\)90046-8](https://doi.org/10.1016/0301-679x(80)90046-8)
- 628 Bowling, D. R., Logan, B. A., Hufkens, K., Aubrecht, D. M., Richardson, A. D., Burns, S. P., et
629 al. (2018). Limitations to winter and spring photosynthesis of a Rocky Mountain subalpine
630 forest. *Agricultural and Forest Meteorology*, 252, 241–255.
631 <https://doi.org/10.1016/j.agrformet.2018.01.025>
- 632 Bunce, A., Volin, J. C., Miller, D. R., Parent, J., & Rudnicki, M. (2019). Determinants of tree
633 sway frequency in temperate deciduous forests of the Northeast United States. *Agricultural*
634 *and Forest Meteorology*, 266–267(December 2018), 87–96.
635 <https://doi.org/10.1016/j.agrformet.2018.11.020>
- 636 Burns, S. P., Blanken, P. D., Turnipseed, A. A., Hu, J., & Monson, R. K. (2015). The influence
637 of warm-season precipitation on the diel cycle of the surface energy balance and carbon
638 dioxide at a Colorado subalpine forest site. *Biogeosciences*, 12(23), 7349–7377.
639 <https://doi.org/10.5194/bg-12-7349-2015>
- 640 Burns, S P. (2018). *The Influence of Warm-Season Precipitation on Water Cycling and the*
641 *Surface Energy Budget Within and Just-Above a Colorado Subalpine Forest in*
642 *Mountainous Terrain: Measurements and Modeling*. University of Colorado, Boulder.
- 643 Burns, Sean P., Swenson, S. C., Wieder, W. R., Lawrence, D. M., Bonan, G. B., Knowles, J. F.,
644 & Blanken, P. D. (2018). A Comparison of the Diel Cycle of Modeled and Measured Latent
645 Heat Flux During the Warm Season in a Colorado Subalpine Forest. *Journal of Advances in*
646 *Modeling Earth Systems*, 10(3), 617–651. <https://doi.org/10.1002/2017MS001248>
- 647 Charrier, G., Charra-Vaskou, K., Legros, B., Améglio, T., & Mayr, S. (2014). Changes in
648 ultrasound velocity and attenuation indicate freezing of xylem sap. *Agricultural and Forest*
649 *Meteorology*, 185, 20–25. <https://doi.org/10.1016/j.agrformet.2013.10.009>
- 650 Charrier, G., Nolf, M., Leitinger, G., Charra-Vaskou, K., Losso, A., Tappeiner, U., et al. (2017).
651 Monitoring of Freezing Dynamics in Trees: A Simple Phase Shift Causes Complexity.
652 *Plant Physiology*, 173(4), 2196–2207. <https://doi.org/10.1104/pp.16.01815>
- 653 Church, J. (1912). The conservation of snow: its dependence on forests and mountains. *Scientific*
654 *American Supplement*, 74, 152–155.
- 655 Ciruzzi, D. M., & Loheide, S. P. (2019). Monitoring Tree Sway as an Indicator of Water Stress.
656 *Geophysical Research Letters*, 46(21), 12021–12029.
657 <https://doi.org/10.1029/2019GL084122>
- 658 Dargahi, M., Newson, T., & Moore, J. R. (2020). A numerical approach to estimate natural
659 frequency of trees with variable properties. *Forests*, 11(9).
660 <https://doi.org/10.3390/F11090915>
- 661 Dickerson-Lange, S. E., Gersonde, R. F., Hubbart, J. A., Link, T. E., Nolin, A. W., Perry, G. H.,
662 et al. (2017). Snow disappearance timing is dominated by forest effects on snow

- 663 accumulation in warm winter climates of the Pacific Northwest, United States.
664 *Hydrological Processes*, 31(10), 1846–1862. <https://doi.org/10.1002/hyp.11144>
- 665 van Emmerik, T., Steele-Dunne, S., Hut, R., Gentine, P., Guerin, M., Oliveira, R., et al. (2017).
666 Measuring Tree Properties and Responses Using Low-Cost Accelerometers. *Sensors*, 17(6),
667 1098. <https://doi.org/10.3390/s17051098>
- 668 van Emmerik, T., Steele-Dunne, S., Gentine, P., Oliveira, R. S., Bittencourt, P., Barros, F., & van
669 de Giesen, N. (2018). Ideas and perspectives: Tree–atmosphere interaction responds to
670 water-related stem variations. *Biogeosciences*, 15(21), 6439–6449.
671 <https://doi.org/10.5194/bg-15-6439-2018>
- 672 Enuş, M., Dellwik, E., Mann, J., Hangan, H., & Costache, A. (2020). Three-dimensional
673 measurements of tree crown movement using an infrared time-of-flight camera.
674 *Experiments in Fluids*, 61(11), 1–13. <https://doi.org/10.1007/s00348-020-03053-y>
- 675 Essery, R., Rutter, N., Pomeroy, J., Baxter, R., Stähli, M., Gustafsson, D., et al. (2009).
676 SNOWMIP2: An Evaluation of Forest Snow Process Simulations. *Bulletin of the American*
677 *Meteorological Society*, 90(8), 1120–1135. <https://doi.org/10.1175/2009BAMS2629.1>
- 678 Evans, J. R., Allen, R. M., Chung, A. I., Cochran, E. S., Guy, R., Hellweg, M., & Lawrence, J. F.
679 (2014). Performance of Several Low-Cost Accelerometers. *Seismological Research Letters*,
680 85(1), 147–158. <https://doi.org/10.1785/0220130091>
- 681 Friesen, J., Lundquist, J., & Van Stan, J. T. (2015). Evolution of forest precipitation water
682 storage measurement methods. *Hydrological Processes*, 29(11), 2504–2520.
683 <https://doi.org/10.1002/hyp.10376>
- 684 Gao, S., Wang, X., Wang, L., & Allison, R. B. (2013). Effect of Temperature on Acoustic
685 Evaluation of Standing Trees and Logs: Part 2: Field Investigation. *Wood and Fiber*
686 *Science*, 45(1), 15–25.
- 687 Gao, S., Wang, X., & Wang, L. (2015). Modeling temperature effect on dynamic modulus of
688 elasticity of red pine (*Pinus resinosa*) in frozen and non-frozen states. *Holzforschung*, 69(2),
689 233–240. <https://doi.org/10.1515/hf-2014-0048>
- 690 Gardiner, B. A. (1992). Mathematical modelling of the static and dynamic characteristics of
691 plantation trees. In J. Franke & A. Roeder (Eds.), *Mathematical Modelling of Forest*
692 *Ecosystems* (pp. 40–61). Sauerländers Verlag, Frankfurt am Main.
- 693 Gerhards, C. (1982). Effect of moisture content and temperature on the mechanical properties of
694 wood: an analysis of immediate effects. *Wood and Fiber Science*, 14(1), 4–36.
- 695 Gougherty, A. V., Keller, S. R., Kruger, A., Stylinski, C. D., Elmore, A. J., & Fitzpatrick, M. C.
696 (2018). Estimating tree phenology from high frequency tree movement data. *Agricultural*
697 *and Forest Meteorology*, 263, 217–224. <https://doi.org/10.1016/j.agrformet.2018.08.020>
- 698 Granucci, D., Rudnicki, M., Hiscox, A., Miller, D., & Su, H.-B. (2013). Quantifying the effects
699 of freezing on tree sway frequencies. *Agricultural and Forest Meteorology*, 168, 10–14.
700 <https://doi.org/10.1016/j.agrformet.2012.07.016>
- 701 Green, D., & Evans, J. (2008). The Immediate Effect of Temperature on the Modulus of
702 Elasticity of Green and Dry Lumber. *Wood and Fiber Science*, 40(3), 374–383.

- 703 Green, D., Evans, J., Logan, J., & Nelson, W. (1999). Adjusting modulus of elasticity of lumber
704 for changes in temperature. *Forest Products Journal*, 49(10), 82–94.
- 705 Guswa, A. J., Tetzlaff, D., Selker, J. S., Carlyle-Moses, D. E., Boyer, E. W., Bruen, M., et al.
706 (2020). Advancing ecohydrology in the 21st century: A convergence of opportunities.
707 *Ecohydrology*, 13(4), 1–14. <https://doi.org/10.1002/eco.2208>
- 708 Gutmann, E. D. (2020). Global modeling of precipitation partitioning by vegetation and their
709 applications. In *Precipitation Partitioning by Vegetation: A Global Synthesis* (pp. 104–119).
710 https://doi.org/10.1007/978-3-030-29702-2_7
- 711 Gutmann, E. D., Van Stan, J. T., Friesen, J., Aubrey, D. P., & Lundquist, J. (2017). Observed
712 compression of in situ tree stems during freezing. *Agricultural and Forest Meteorology*,
713 243, 19–24. <https://doi.org/10.1016/j.agrformet.2017.05.004>
- 714 Harpold, A. A., Guo, Q., Molotch, N., Brooks, P. D., Bales, R., Fernandez-Diaz, J. C., et al.
715 (2014). LiDAR-derived snowpack data sets from mixed conifer forests across the Western
716 United States. *Water Resources Research*, 50. <https://doi.org/10.1002/2013WR013935>
- 717 Hassinen, A., Lemettinen, M., Peltola, H., Kellomäki, S., & Gardiner, B. (1998). A prism-based
718 system for monitoring the swaying of trees under wind loading. *Agricultural and Forest
719 Meteorology*, 90(3), 187–194. [https://doi.org/10.1016/S0168-1923\(98\)00052-5](https://doi.org/10.1016/S0168-1923(98)00052-5)
- 720 Hedstrom, N. R., & Pomeroy, J. W. (1998). Measurements and modelling of snow interception
721 in the boreal forest. *Hydrol. Processes*, 12, 1611–1625.
- 722 Jackson, T., Shenkin, A., Moore, J., Bunce, A., van Emmerik, T., Kane, B., et al. (2019). An
723 architectural understanding of natural sway frequencies in trees. *Journal of The Royal
724 Society Interface*, 16(20190116). <https://doi.org/10.1098/rsif.2019.0116>
- 725 Jackson, T. D., Sethi, S., Dellwik, E., Angelou, N., Bunce, A., van Emmerik, T., et al. (2021).
726 The motion of trees in the wind: a data synthesis. *Biogeosciences*, 18(13), 4059–4072.
727 <https://doi.org/10.5194/bg-18-4059-2021>
- 728 Kinar, N. J., & Pomeroy, J. W. (2015). Measurement of the physical properties of the snowpack.
729 *Reviews of Geophysics*, 53(2), 481–544. <https://doi.org/10.1002/2015RG000481>
- 730 Klamerus-Iwan, A., Link, T. E., Keim, R. F., & Van Stan II, J. T. (2020). Storage and Routing of
731 Precipitation Through Canopies. In J. T. Van Stan II, E. Gutmann, & J. Friesen (Eds.),
732 *Precipitation Partitioning by Vegetation: A Global Synthesis* (pp. 17–34). Cham: Springer
733 International Publishing. https://doi.org/10.1007/978-3-030-29702-2_2
- 734 Kobayashi, D. (1987). Snow accumulation on a narrow board. *Cold Regions Science and
735 Technology*, 13(3), 239–245. [https://doi.org/10.1016/0165-232X\(87\)90005-X](https://doi.org/10.1016/0165-232X(87)90005-X)
- 736 Kooreman, B. (2013). *Measuring weight fluctuations in trees based on natural frequency*. Delft
737 University of Technology.
- 738 Lindfors, L., Atherton, J., Riikonen, A., & Hölttä, T. (2019). A mechanistic model of winter stem
739 diameter dynamics reveals the time constant of diameter changes and the elastic modulus
740 across tissues and species. *Agricultural and Forest Meteorology*, 272–273, 20–29.
741 <https://doi.org/10.1016/j.agrformet.2019.03.016>
- 742 Lundquist, J. D., Dickerson-Lange, S. E., Lutz, J. A., & Cristea, N. C. (2013). Lower forest

- 743 density enhances snow retention in regions with warmer winters: A global framework
744 developed from plot-scale observations and modeling. *Water Resources Research*, 49.
745 <https://doi.org/10.1002/wrcr.20504>
- 746 Lundquist, J. D., Dickerson-Lange, S., Gutmann, E., Jonas, T., Lumbrazo, C., & Reynolds, D.
747 (2021). Snow interception modeling: Isolated observations have led to many land surface
748 models lacking appropriate temperature sensitivities. *Hydrological Processes*.
749 <https://doi.org/10.1002/hyp.14274>
- 750 Lv, Z., & Pomeroy, J. W. (2019). Detecting intercepted snow on mountain needleleaf forest
751 canopies using satellite remote sensing. *Remote Sensing of Environment*, 231(111222), 1–
752 19. <https://doi.org/10.1016/j.rse.2019.111222>
- 753 Lv, Z., & Pomeroy, J. W. (2020). Assimilating snow observations to snow interception process
754 simulations. *Hydrological Processes*, 1–18. <https://doi.org/10.1002/hyp.13720>
- 755 Martin, K. A., Van Stan, J. T., Dickerson-Lange, S. E., Lutz, J. A., Berman, J. W., Gersonde, R.,
756 & Lundquist, J. D. (2013). Development and testing of a snow interceptometer to quantify
757 canopy water storage and interception processes in the rain/snow transition zone of the
758 North Cascades, Washington, USA. *Water Resources Research*, 49.
759 <https://doi.org/10.1002/wrcr.20271>
- 760 Mayhead, G. J. (1973). Sway periods of forest trees. *Scottish Forestry*, 27(1), 19–23.
- 761 Miller, D. H. (1962). Snow in the trees – where does it go? In *Proc. 30th Western Snow*
762 *Conference* (pp. 21–27). Cheyenne.
- 763 Moeser, D., Mazzotti, G., Helbig, N., & Jonas, T. (2016). Representing spatial variability of
764 forest snow: Implementation of a new interception model. *Water Resources Research*, 52.
765 <https://doi.org/10.1002/2015WR017961>
- 766 Molotch, N. P., Blanken, P. D., Williams, M. W., Turnipseed, A. A., Monson, R. K., &
767 Margulis, S. A. (2007). Estimating sublimation of intercepted and sub-canopy snow using
768 eddy covariance systems. *Hydrological Processes*, 21(12), 1567–1575.
769 <https://doi.org/10.1002/hyp.6719>
- 770 Montesi, J., Elder, K., Schmidt, R. A., & Davis, R. E. (2004). Sublimation of Intercepted Snow
771 within a Subalpine Forest Canopy at Two Elevations. *Journal of Hydrometeorology*, 5(5),
772 763–773. [https://doi.org/10.1175/1525-7541\(2004\)005<0763:SOISWA>2.0.CO;2](https://doi.org/10.1175/1525-7541(2004)005<0763:SOISWA>2.0.CO;2)
- 773 Moore, J. R., & Maguire, D. A. (2004). Natural sway frequencies and damping ratios of trees:
774 concepts, review and synthesis of previous studies. *Trees - Structure and Function*, 18(2),
775 195–203. <https://doi.org/10.1007/s00468-003-0295-6>
- 776 Musselman, K. N., & Pomeroy, J. W. (2017). Estimation of Needleleaf Canopy and Trunk
777 Temperatures and Longwave Contribution to Melting Snow. *Journal of Hydrometeorology*,
778 18(2), 555–572. <https://doi.org/10.1175/JHM-D-16-0111.1>
- 779 Musselman, K. N., Molotch, N. P., & Brooks, P. D. (2008). Effects of vegetation on snow
780 accumulation and ablation in a mid-latitude sub-alpine forest. *Hydrological Processes*,
781 22(15), 2767–2776. <https://doi.org/10.1002/hyp.7050>
- 782 Nakai, Y., Sakamoto, T., Terajima, T., Kitahara, H., & Saito, T. (1994). Snow interception by
783 forest canopies: weighing a conifer tree, meteorological observation and analysis by the

- 784 Penman-Monteith formula. In *Snow and Ice Covers: Interactions with the Atmosphere*
785 *Ecosystems, IAHS Publ. no. 223* (pp. 227–236).
- 786 Onwona-Agyeman, S., Morioka, N., Kondo, M., & Kitagawa, K. (1995). Seasonal changes in the
787 Modulus of Elasticity of living branches of three coniferous species. *Ecological Research*,
788 *10*(2), 199–206. <https://doi.org/10.1007/BF02347942>
- 789 Papesch, A. J. . (1984). *Wind and its effects on (Canterbury) forests. University of Canterbury.*
790 University of Canterbury.
- 791 Peltola, H. (1996). Swaying of trees in response to wind and thinning in a stand of Scots pine.
792 *Boundary-Layer Meteorology*, *77*(3–4), 285–304. <https://doi.org/10.1007/BF00123529>
- 793 Pivato, D., Dupont, S., & Brunet, Y. (2014). A simple tree swaying model for forest motion in
794 windstorm conditions. *Trees - Structure and Function*, *28*, 281–293.
795 <https://doi.org/10.1007/s00468-013-0948-z>
- 796 Pomeroy, J.W., & Dion, K. (1996). Winter radiation extinction and reflection in a boreal pine
797 canopy: measurements and modelling. *Hydrological Processes*, *10*(12), 1591–1608.
798 [https://doi.org/10.1002/\(SICI\)1099-1085\(199612\)10:12<1591::AID-HYP503>3.0.CO;2-8](https://doi.org/10.1002/(SICI)1099-1085(199612)10:12<1591::AID-HYP503>3.0.CO;2-8)
- 799 Pomeroy, John W., & Schmidt, R. A. (1993). The use of fractal geometry in modelling
800 intercepted snow accumulation and sublimation. In *Proc. 50th Eastern Snow Conference*
801 (pp. 1–10). Quebec City.
- 802 Raleigh, M. S. (2021a). Multi-year measurements of tree motion from an accelerometer on a fir
803 tree near Niwot Ridge, Colorado. <https://doi.org/10.5281/zenodo.5149308>
- 804 Raleigh, M. S. (2021b). Multi-year measurements of tree motion from an accelerometer on a
805 spruce tree near Niwot Ridge, Colorado. <https://doi.org/10.5281/zenodo.5130616>
- 806 Raleigh, M. S., Rittger, K., Moore, C. E., Henn, B., Lutz, J. A., & Lundquist, J. D. (2013).
807 Ground-based testing of MODIS fractional snow cover in subalpine meadows and forests of
808 the Sierra Nevada. *Remote Sensing of Environment*, *128*, 44–57.
809 <https://doi.org/10.1016/j.rse.2012.09.016>
- 810 Richardson, A. D., Hufkens, K., Milliman, T., Aubrecht, D. M., Chen, M., Gray, J. M., et al.
811 (2018). Tracking vegetation phenology across diverse North American biomes using
812 PhenoCam imagery. *Scientific Data*, *5*, 180028. <https://doi.org/10.1038/sdata.2018.28>
- 813 Roth, T. R., & Nolin, A. W. (2019). Characterizing Maritime Snow Canopy Interception in
814 Forested Mountains. *Water Resources Research*, *55*(6), 4564–4581.
815 <https://doi.org/10.1029/2018WR024089>
- 816 Russell, M., U. H. Eitel, J., J. Maguire, A., & E. Link, T. (2020). Toward a Novel Laser-Based
817 Approach for Estimating Snow Interception. *Remote Sensing*, *12*(7), 1146.
818 <https://doi.org/10.3390/rs12071146>
- 819 Rutter, N., Essery, R., Pomeroy, J., Altimir, N., Andreadis, K., Baker, I., et al. (2009). Evaluation
820 of forest snow processes models (SnowMIP2). *Journal of Geophysical Research*, *114*, 1–
821 18. <https://doi.org/10.1029/2008JD011063>
- 822 Schmidt, R. A., & Gluns, D. R. (1991). Snowfall interception on branches of three conifer
823 species. *Canadian Journal of Forest Research*, *21*(8), 1262–1269.

- 824 <https://doi.org/10.1139/x91-176>
- 825 Schmidt, R. A., & Pomeroy, J. W. (1990). Bending of a conifer branch at subfreezing
826 temperatures: implications for snow interception. *Canadian Journal of Forest Research*,
827 20(8), 1251–1253. <https://doi.org/10.1139/x90-165>
- 828 Selker, J. S., Lane, J. W., Rupp, D. E., Hut, R., Abou Najm, M. R., Stewart, R. D., et al. (2011).
829 The answer is blowing in the wind: using wind induced resonance of trees to measure time
830 varying canopy mass, including interception. In *AGU Fall Meeting*. #H11G-1155.
- 831 Silins, U., Lieffers, V. J., & Bach, L. (2000). The effect of temperature on mechanical properties
832 of standing lodgepole pine trees. *Trees*, 14(8), 424–428.
833 <https://doi.org/10.1007/s004680000065>
- 834 Van Stan, J. T., Martin, K. A., Friesen, J., Jarvis, M. T., Lundquist, J. D., & Levia, D. F. (2013).
835 Evaluation of an instrumental method to reduce error in canopy water storage estimates via
836 mechanical displacement. *Water Resources Research*, 49(1), 54–63.
837 <https://doi.org/10.1029/2012WR012666>
- 838 Storck, P., Lettenmaier, D., & Bolton, S. (2002). Measurement of snow interception and canopy
839 effects on snow accumulation and melt in a mountainous maritime climate, Oregon, United
840 States. *Water Resources Research*, 38(11), 1–16.
- 841 Sugden, M. J. (1962). Tree sway period - a possible new parameter for crown classification and
842 stand competition. *The Forestry Chronicle*, 38(3), 336–344.
843 <https://doi.org/10.5558/tfc38336-3>
- 844 Sun, Y., Zhou, H., Shan, G., Grantz, D. A., Schulze Lammers, P., Xue, X., et al. (2019). Diurnal
845 and seasonal transitions of water and ice content in apple stems: Field tracking the radial
846 location of the freezing- and thawing-fronts using a noninvasive smart sensor. *Agricultural
847 and Forest Meteorology*, 274(February), 75–84.
848 <https://doi.org/10.1016/j.agrformet.2019.04.018>
- 849 Turnipseed, A. A., Blanken, P. D., Anderson, D. E., & Monson, R. K. (2002). Energy budget
850 above a high-elevation subalpine forest in complex topography. *Agricultural and Forest
851 Meteorology*, 110(3), 177–201. [https://doi.org/10.1016/S0168-1923\(01\)00290-8](https://doi.org/10.1016/S0168-1923(01)00290-8)
- 852 USDA Forest Service. (2010). *Wood Handbook*. (R. J. Ross, Ed.), *General Technical Report
853 FPL-GTR-190*. Madison: USDA Forest Service Forest Products Laboratory.
- 854 Varhola, A., Coops, N. C., Weiler, M., & Moore, R. D. (2010). Forest canopy effects on snow
855 accumulation and ablation: An integrative review of empirical results. *Journal of
856 Hydrology*, 392(3–4), 219–233. <https://doi.org/10.1016/j.jhydrol.2010.08.009>
- 857 Yang, Z., Hui, K. W., Abbas, S., Zhu, R., Kwok, C. Y. T., Heo, J., et al. (2021). A Review of
858 Dynamic Tree Behaviors: Measurement Methods on Tree Sway, Tree Tilt, and Root–Plate
859 Movement. *Forests*, 12(3), 379. <https://doi.org/10.3390/f12030379>
- 860

1

2

Water Resources Research

3

Supporting Information for

4

Challenges and Capabilities in Estimating Snow Mass Intercepted in Conifer Canopies

5

with Tree Sway Monitoring

6

Mark S. Raleigh¹, Ethan D. Gutmann², John T. Van Stan II³, Sean Burns^{2,4}, Peter Blanken⁴, and Eric

7

E. Small⁵

8

¹College of Earth, Ocean, and Atmospheric Sciences, Oregon State University, Corvallis, OR,

9

USA.

10

²National Center for Atmospheric Research, Boulder, CO, USA.

11

³Department of Biological, Geological, and Environmental Sciences, Cleveland State University,

12

Cleveland, OH, USA.

13

⁴Department of Geography, University of Colorado, Boulder, CO, USA.

14

⁵Department of Geological Sciences, University of Colorado, Boulder, CO, USA.

15

16

Contents of this file

17

18

Text S1 to S5

19

Figures S1 to S11

20

Tables S1 to S4

21

22

Introduction

23

This supporting information document includes additional details on (1) the accelerometer

24

installation and study trees, (2) the dependence of tree sway on temperature and the

25

independence of tree sway from wind speed, (3) the effect of window size on derived tree

26

sway frequency, (4) the estimation of thermal effects on tree sway with different temperature

27

datasets, and (5) the conversion of changes in tree sway to changes in mass.

28 **Text S1. Additional details on accelerometer installation**

29 The Gulf Coast Data Concepts (GCDC) accelerometers were weatherproofed in plastic wrap
30 and installed on the north side of each study tree. Magnetic north was used as the reference
31 using a compass, though the sensors were not precisely oriented to north. The USB port of
32 each GCDC sensor was oriented toward the ground. Given this configuration, the sensor “X-
33 axis” was the vertical axis, while the “Y-axis” (east-west motion) and “Z-axis” (north-south
34 motion) were the lateral axes (see GCDC X16-1D user manual, dated March 22, 2016, available
35 at http://www.gcdadataconcepts.com/GCDC_X16-1D_User_Manual.pdf). The installation height
36 and basic tree measurements are shown in Table S1.

37
38 For each GCDC accelerometer, data were stored on an internal memory card and were
39 downloaded manually by unplugging the USB cable from the power supply at the access port
40 (Fig. 3c in main text) and connecting to a field laptop. After download, the memory card was
41 cleared, the time/date corrected for drift (typically negligible), and the USB was reconnected
42 to the power source to resume data logging.

43
44 The GCDC accelerometer has an on-board AA battery (Fig. 3a in main text), which was
45 insufficient to ensure long-term monitoring of tree sway. We provided external power from a
46 nearby datalogger to each accelerometer via the USB extension and a 12V to 5V USB DC
47 Converter (manufacturer: Autotek).

48
49 **Text S2. Comparisons of seasonal temperature and wind speed to tree sway**

50 Time series of hourly air temperature (Figure S1), bole temperature (Figures S2-S3), and wind
51 speed (Figure S4) are included for additional interpretation of the tree sway time series (Figure
52 6 in main text). A direct comparison of tree sway versus air temperature and wind speed is
53 shown in Figure S5. This illustrates the seasonality of tree sway with higher sway frequency at
54 lower temperatures (typically in the winter months) and lower sway frequency at higher
55 temperatures (typically in the summer months) (Fig. S5a,c).

56
57 In contrast to temperature, wind speed shows lower correspondence to the sway frequency
58 data (Fig. S5b,d). A given wind speed may yield wide range of sway frequency values, which
59 reinforces that sway frequency does not depend on the magnitude of wind speed but rather
60 on tree properties related to mass, rigidity, and geometry (see Equation 1 in main text).
61 Although lower sway frequency and wind speeds are found in summer, and higher sway
62 frequency and higher wind speeds are found in winter, the relationship is not casual. The main
63 dependence on observed tree sway frequency and wind speed is that there appears to be a
64 threshold wind speed required to induce tree movement (note gap at the left side of the data
65 near 0 m s^{-1} in Fig. S5b,d). For the spruce tree, 99% of the detected tree sway values had a
66 mean hourly wind speed of at least 1.26 m s^{-1} , while 99.9% had a mean hourly wind speed of at
67 least 0.56 m s^{-1} . For the fir tree, 99% of the detected tree sway values had a mean hourly wind
68 speed of at least 0.96 m s^{-1} , while 99.9% had a mean hourly wind speed of at least 0.26 m s^{-1} .
69 The tree-to-tree differences in these wind speed thresholds necessary to initiate sway motion
70 may be due to the difference in tree size (i.e., the spruce is larger and may require higher wind
71 speed to set into motion).

72
73 Although the tree sway frequency does not depend on wind speed (assuming it is above the
74 threshold for movement initiation), the variations in hourly tree movement scale directly with

75 wind energy (Figure S6 and Figure 4a in main text). Here, the variations in tree movement are
76 characterized with the standard deviation in lateral acceleration, while wind energy is the
77 squared wind speed. A higher squared wind speed causes greater variations in tree motion
78 (i.e., more chaotic), which should be readily understood. This figure is tangential to the main
79 analysis (which focuses on tree sway frequency, not the standard deviation in tree
80 acceleration), but is included to convey the manner in which tree motion responds to wind
81 speed.
82

83 **Text S3. Selection of window length for frequency analysis**

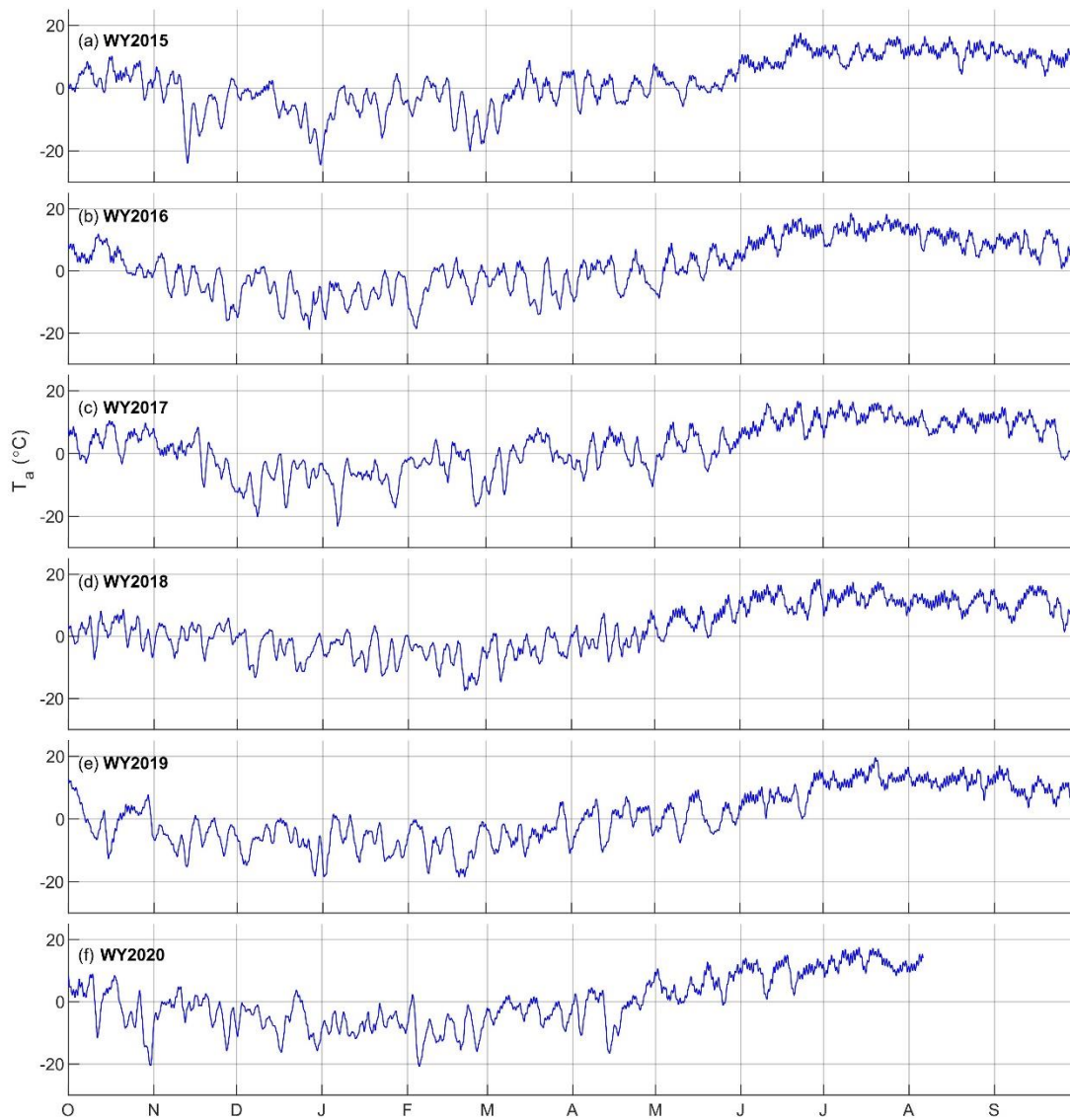
84 In the main analysis, we conducted frequency analysis on the 12 Hz accelerometer data to
85 identify a sway frequency over a window length of 1 hour (60 minutes). We tested whether
86 selection of a narrower window (5 minutes) would significantly alter the analysis. For this
87 analysis, we only present data from one lateral axis on the spruce tree over mid-winter in
88 water year 2017 (Figures S7-S8). Similar tree sway values were found for both window sizes (5
89 minute and 60 minute), but the 5-minute window produced additional noise at short time
90 scales and sporadic larger variations from the prevailing values. We did not assess the
91 mechanism behind these sporadic deviations in 5-minute tree sway. The sway values were in
92 close agreement (Figure S8), regardless of whether a 60-minute window was used for the
93 frequency analysis or a 5-minute window was used (and all 5-minute values averaged to a 60-
94 minute value). These comparisons supported our selection of a 60-minute window for the
95 main frequency analysis, as it reduced noise relative to the 5-minute window, while yielding
96 similar central values.
97

98 **Text S4. Estimation of unloaded sway with tree bole temperature versus air temperature**

99 We fit Equation 4 (see main text) to a subset of points ($n=1000$) when snow was known to be
100 absent from the forest canopy. This fit was done separately for each water year to control for
101 changes in sway frequency due to tree growth. In developing the fit, we evaluated use of both
102 hourly bole temperatures and 36-hour smoothed air temperatures. The fit of Equation 4 for
103 each year, temperature dataset, and tree are shown in Figures S9-S10. The derived parameters
104 and fit statistics are shown in Tables S2-S3. Similar skill metrics were achieved regardless of
105 which temperature dataset was used to fit the model. For the spruce tree, the bole
106 temperature yielded improved statistics in three out of the five water years when both
107 temperature datasets were available. For the fir tree, the air temperature yielded improved
108 statistics in four out of the five years. The standard deviation in the residuals of the fit varied
109 with temperature (Figure S11), which was accounted for in the calculation of the signal-to-
110 noise (SNR) threshold used to detect the snow interception signal (see main text).
111

112 **Text S5. Estimation of changes in mass from changes in tree sway**

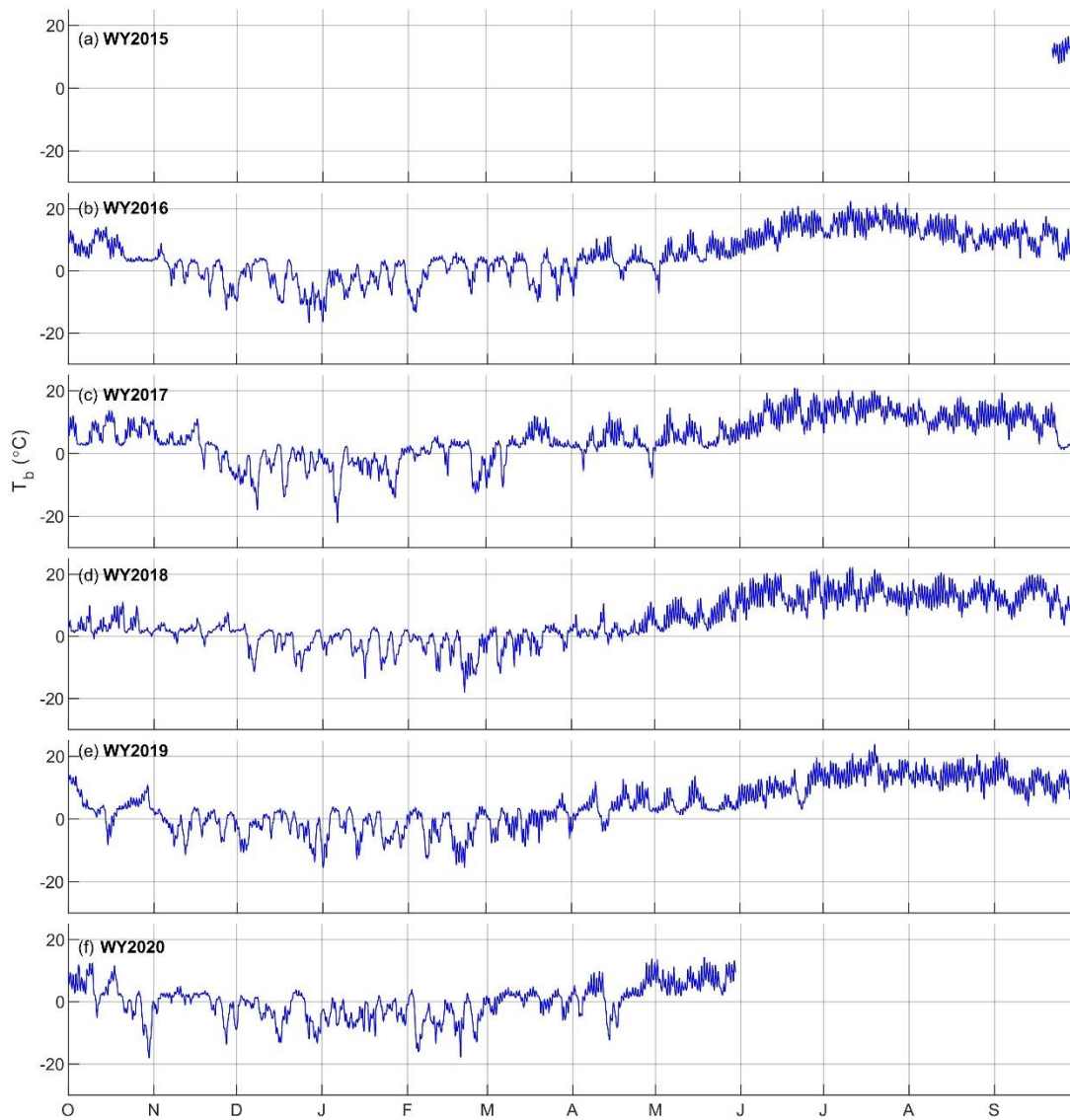
113 Sway tests were used to determine the slope parameter in Equation 7 (see main text) for each
114 tree. The fitted parameter (with 95% confidence intervals) and statistics are shown in Table S4.
115 Note that the equation assumes linearity and that the largest snow masses intercepted in the
116 canopy exceeded the upper limit of masses used in the sway tests. Additionally, the sway tests
117 were conducted with mass at only a single height near the accelerometer (Table S1).
118



119

120 **Figure S1.** Hourly air temperature (36-hour smoothed) measured at 8m height on the US-NR1
 121 AmeriFlux tower over water years (WY) 2015-2020.

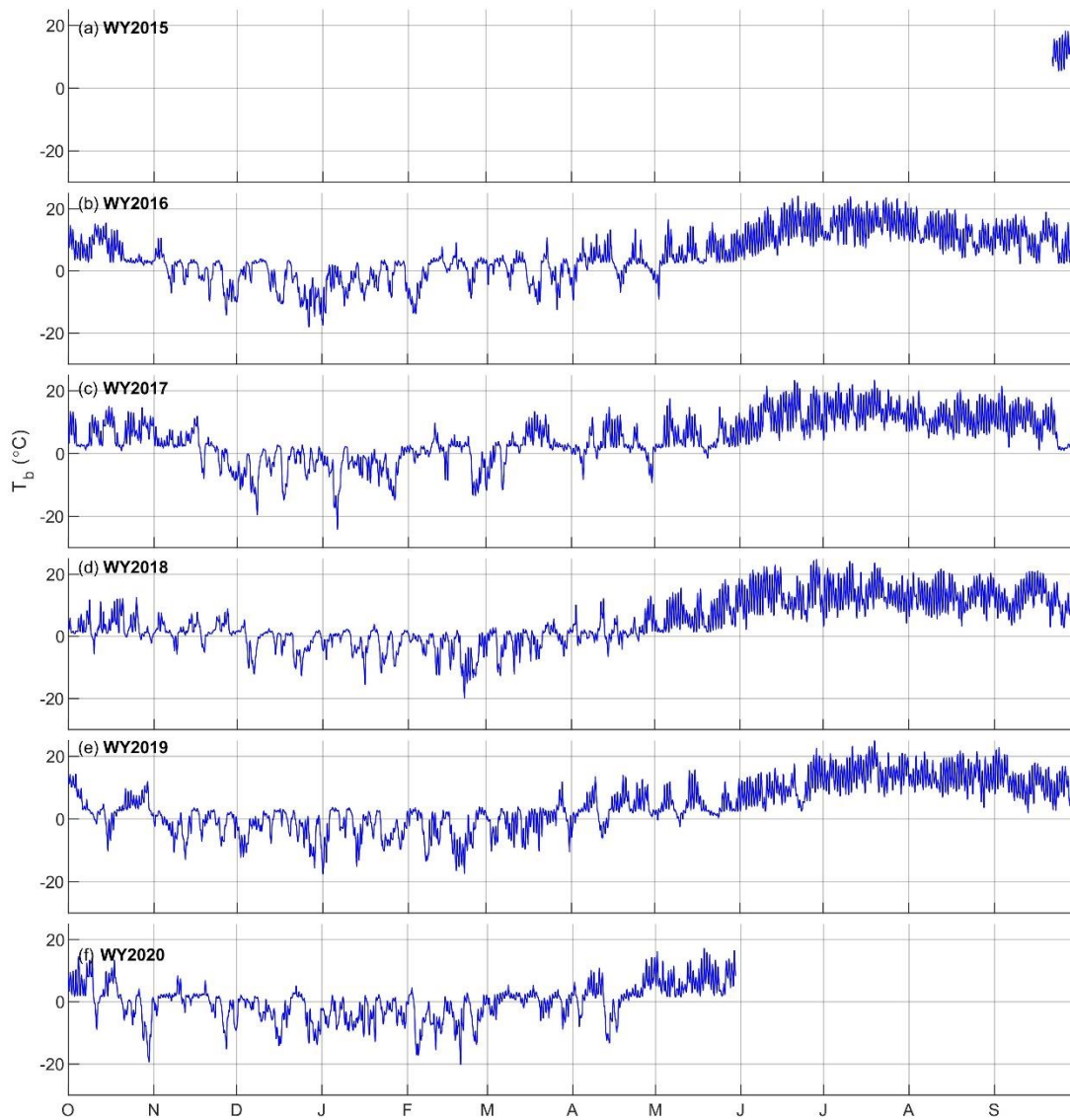
122



123

124 **Figure S2.** Hourly tree bole temperature from a spruce tree near the US-NR1 AmeriFlux tower
 125 over water years (WY) 2015-2020.

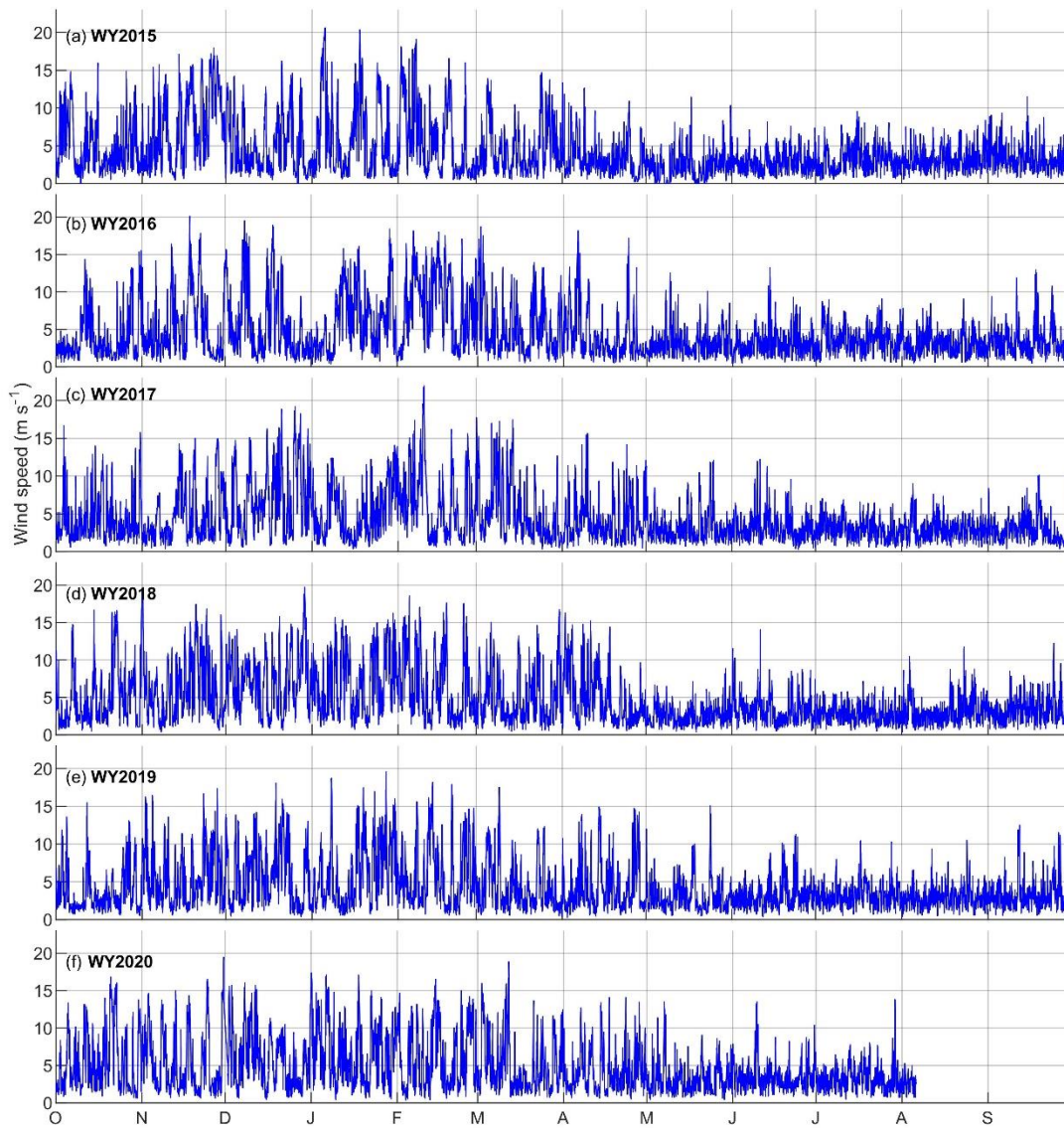
126



127

128 **Figure S3.** Hourly tree bole temperature from a fir tree near the US-NR1 AmeriFlux tower over
 129 water years (WY) 2015-2020.

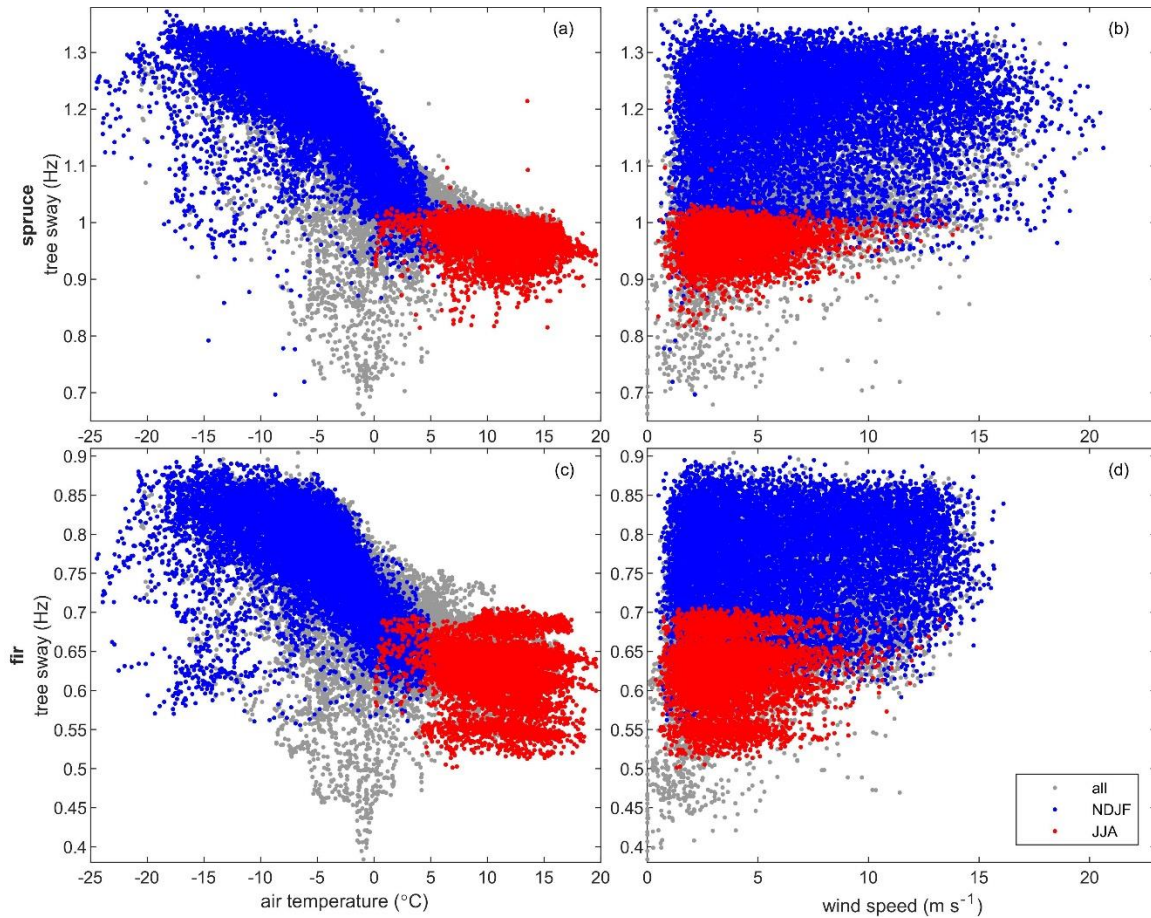
130



131

132 **Figure S4.** Hourly wind speed measured at 21m height on the US-NR1 AmeriFlux tower over
133 water years (WY) 2015-2020.

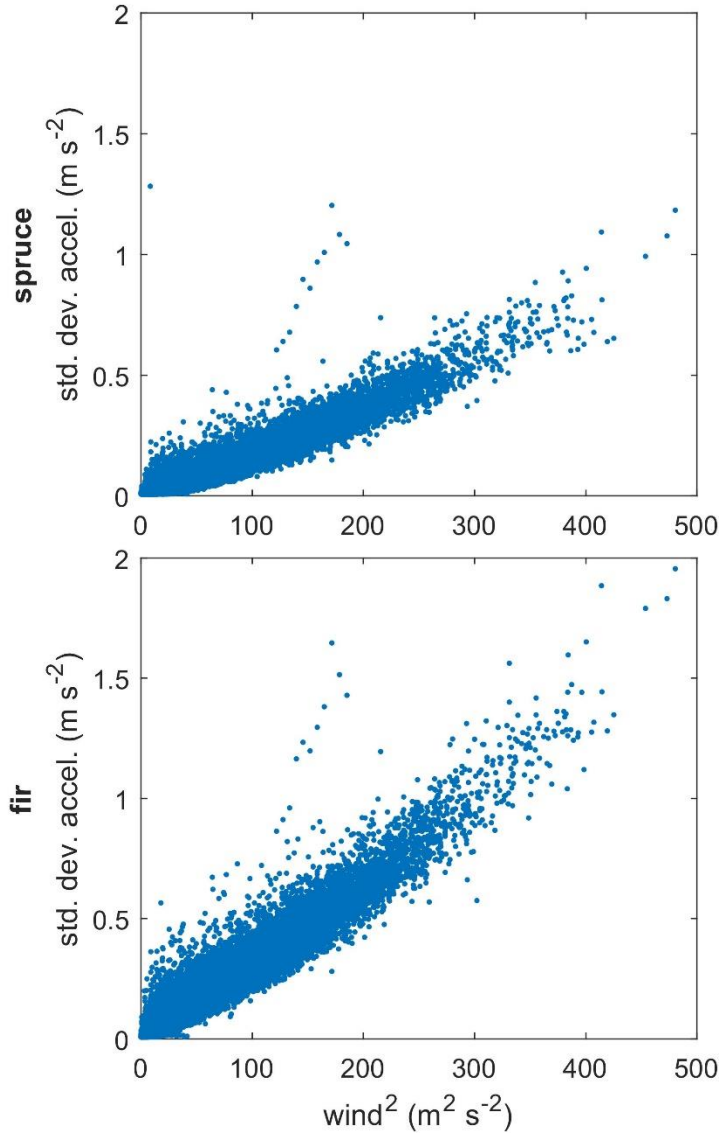
134



135

136 **Figure S5.** Comparison of hourly observations of tree sway and (left) air temperature
 137 (smoothed over 36 hour window) and (right) wind speed for the (top) spruce and (bottom) fir
 138 with all data shown in the study period (November 2014 – August 2020). Points are colored
 139 blue for winter months (November-February, NDHF) and red for summer months (June-
 140 August, JJA). This figure shows that tree sway frequency varies with temperature but is
 141 independent of wind speed. The tree sway data are from the east-west axis, and after filtering
 142 but before smoothing in time.

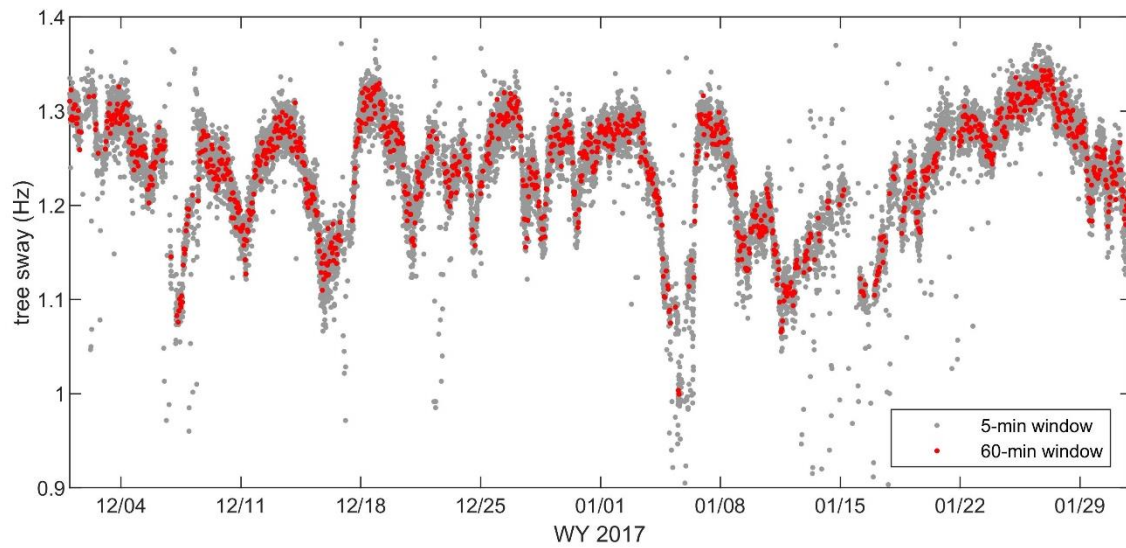
143



144

145 **Figure S6.** Comparison of hourly values of squared wind speed versus standard deviation in
 146 lateral tree acceleration for the (a) spruce and (b) fir over the study period (November 2014 –
 147 August 2020). The acceleration data are from the east-west axis.

148

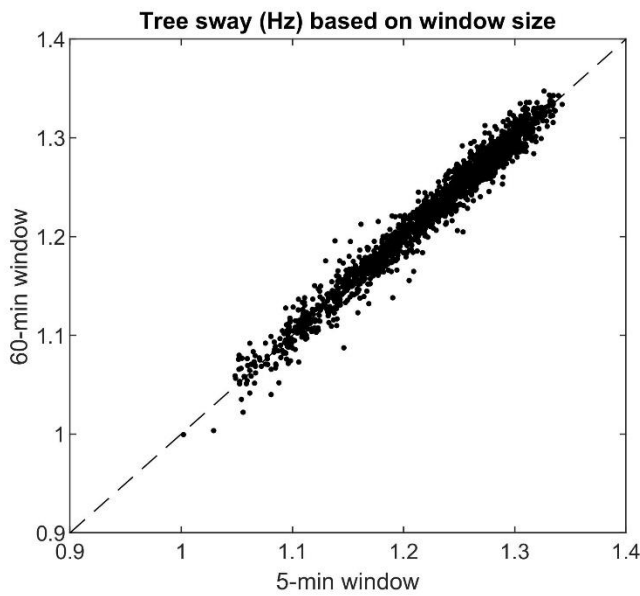


149

150 **Figure S7.** Time series of tree sway derived from acceleration data using a 60-minute window
 151 (red dots) versus a 5-minute window (gray dots). Example data shown are from the east-west
 152 axis of the spruce tree in December-January in water year (WY) 2017. The analysis in the main
 153 text used a 60-minute window (i.e., hourly).

154

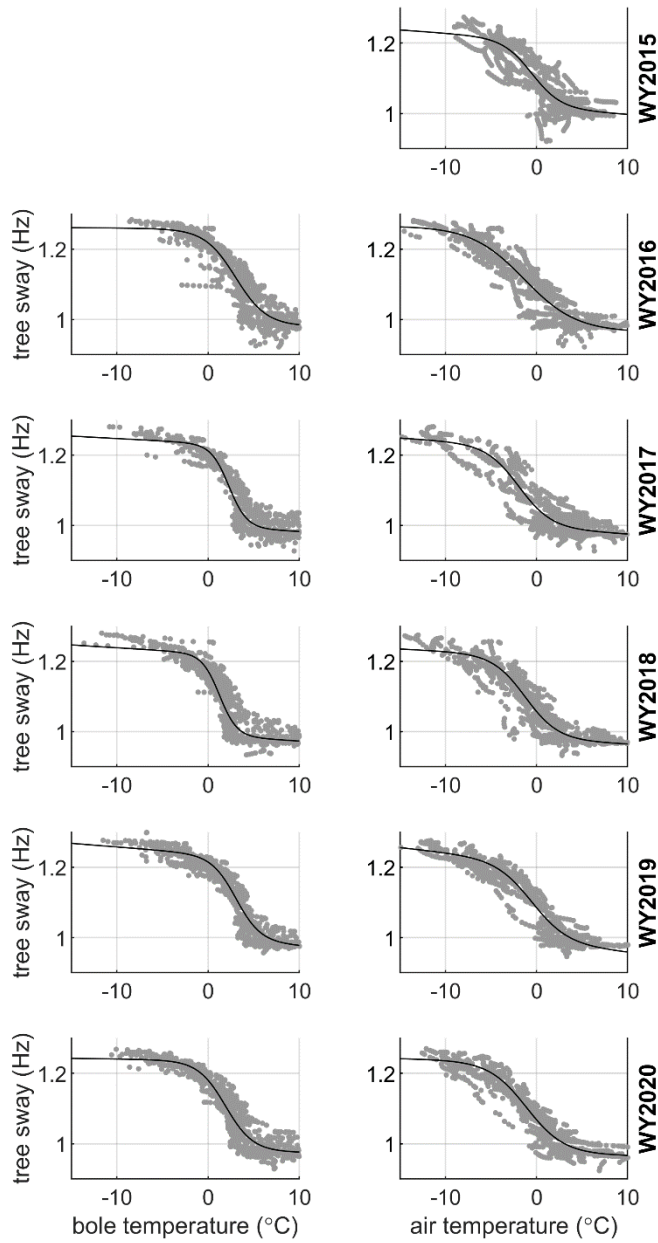
155



156

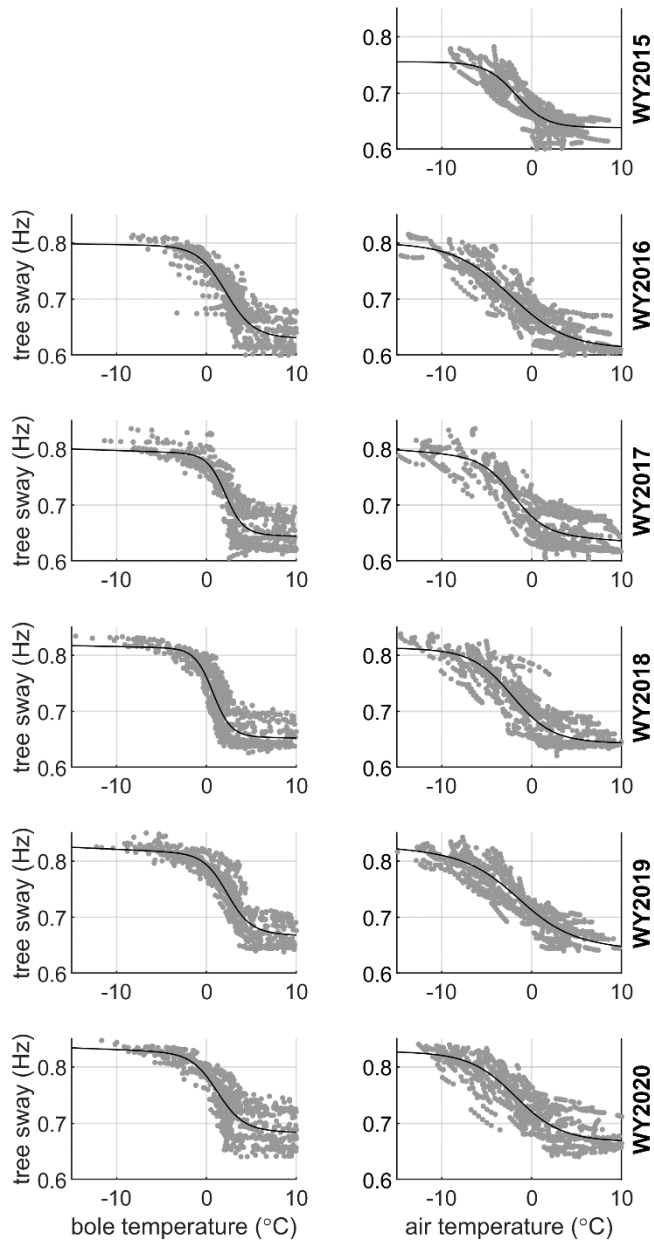
157 **Figure S8.** Scatterplot of tree sway derived from acceleration data using a 60-minute window
 158 versus a 5-minute window. All 5-minute sway values in each 60-minute period are averaged to
 159 facilitate the comparison. Example data are from the east-west axis of the spruce tree in from
 160 late November to early March in water year (WY) 2017.

161



162

163 **Figure S9.** Hourly observed tree sway frequency versus (left) bole temperatures and (right) 36-
 164 hr smoothed air temperatures across the six water years (rows), for the Niwot spruce tree. The
 165 gray markers are the points (n=1000) used to fit the model (black line, Equation 4 in main text).
 166



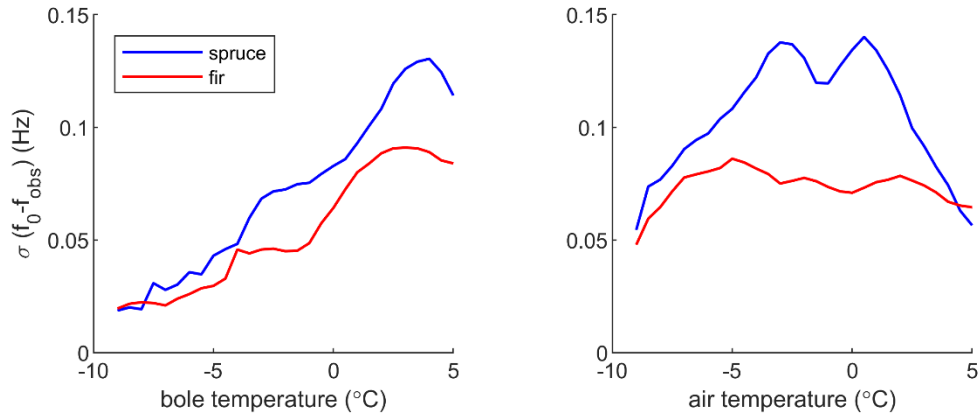
167

168 **Figure S10.** Same as Figure S9 but for the Niwot fir tree.

169

170

171



172

173 **Figure S11.** Standard deviation in the residuals ($f_0 - f_{obs}$) of the Equation 4 fit across all years,
 174 versus (left) bole temperatures and (right) 36-hr smoothed air temperatures for the spruce
 175 (blue) and fir (red). Values are computed over a sliding 2°C window.

176

177

178 **Table S1.** Characteristics of trees instrumented with accelerometers (DBH = diameter at breast
 179 height). Tree characteristics were measured in summer 2017.

Species	DBH (cm)	Crown dia. (m)	Canopy bottom height (m)	Tree Height (m)	Accelerometer Height (m)
Engelmann spruce	35.7	3.4	2.8	13.0	8.9
Subalpine fir	18.5	1.7	2.3	11.0	8.1

180

181 **Table S2.** Parameters fit to Equation 4 for the spruce tree each year, reported separately for
 182 the bole and 36-hr smoothed air temperature datasets, along with fit statistics.

Water year	Temperature source	Curve parameters				h	Statistics	
		a	b	c	d		R^2	RMSE (Hz)
2015	bole	--	--	--	--	--	--	--
	air	1.016	0.6245	1.209	0.3236	0.00187	0.793	0.037
2016	bole	0.9831	0.5889	1.258	-1.773	0.000226	0.894	0.032
	air	0.9637	0.3463	1.266	0.4744	2.22e-14	0.880	0.033
2017	bole	0.9965	1.007	1.233	-2.292	0.00139	0.890	0.032
	air	0.9919	0.5569	1.224	1.088	0.00166	0.874	0.033
2018	bole	0.9895	1.039	1.223	-1.287	0.00161	0.881	0.033
	air	0.9772	0.5538	1.217	0.6826	0.00125	0.899	0.030
2019	bole	0.9970	0.7393	1.237	-2.263	0.00206	0.947	0.023
	air	0.9858	0.5053	1.214	0.2634	0.00280	0.916	0.029
2020	bole	0.9791	0.6639	1.237	-1.262	0.000371	0.919	0.027
	air	0.9715	0.4841	1.233	0.5358	0.000553	0.925	0.027

183 **Table S3.** Same as Table S2 but for the fir tree.

Water year	Temperature source	Curve parameters				<i>h</i>	Statistics	
		<i>a</i>	<i>b</i>	<i>c</i>	<i>d</i>		<i>R</i> ²	<i>RMSE (Hz)</i>
2015	bole	--	--	--	--	--	--	--
	air	0.6389	0.5944	0.7553	1.035	2.22e-14	0.761	0.021
2016	bole	0.6329	0.6459	0.7947	-1.374	0.000236	0.785	0.026
	air	0.6122	0.3161	0.8002	0.7431	2.22e-14	0.805	0.025
2017	bole	0.6497	0.9917	0.7918	-2.076	0.000522	0.750	0.029
	air	0.6476	0.5655	0.7813	1.138	0.00113	0.756	0.029
2018	bole	0.6558	0.9983	0.8119	-0.7124	0.000324	0.794	0.026
	air	0.6459	0.4509	0.8088	0.9856	0.000245	0.836	0.024
2019	bole	0.6750	0.7649	0.8137	-1.754	0.000712	0.868	0.021
	air	0.6565	0.3489	0.8063	0.5048	0.00111	0.848	0.022
2020	bole	0.6898	0.6943	0.8248	-0.8224	0.000611	0.720	0.029
	air	0.6705	0.3990	0.8237	0.7126	0.000237	0.768	0.027

184 **Table S4.** Parameters fit to Equation 7 for the two study trees, along with fit statistics.

Study tree	n	α parameter ($\text{kg Hz}^{-1} \Delta f$) (95% confidence intervals)	Statistics	
			<i>R</i> ²	<i>RMSE (kg Hz⁻¹ Δf)</i>
spruce	12	1092.4 (970.1, 1215)	0.801	6.3
fir	18	321.9 (330.6, 343.3)	0.918	4.1

185